Forschungszentrum Karlsruhe
in der Helmholtz-Gemeinschaft

Wissenschaftliche Berichte
FZKA 6972

In-core and Out-of-core Materials Selection for the HPLWR

K. Ehrlich, J. Konys, L. Heikinheimo, S. Leistikow, H. Steiner, P. Arnoux, M. Schirra

Institut für Materialforschung

Mai 2004

Forschungszentrum Karlsruhe

in der Helmholtz-Gemeinschaft

Wissenschaftliche Berichte

FZKA 6972

In-core and Out-of-core Materials Selection for the HPLWR

K. Ehrlich, J. Konys, L. Heikinheimo*,
S. Leistikow, H. Steiner, P. Arnoux**, M. Schirra

Institut für Materialforschung

*VTT-Espo, Finland
**CEA-Saclay, France

Forschungszentrum Karlsruhe GmbH, Karlsruhe
2004

Impressum der Print-Ausgabe:

Als Manuskript gedruckt

Forschungszentrum Karlsruhe GmbH
Postfach 3640, 76021 Karlsruhe

Mitglied der Hermann von Helmholtz-Gemeinschaft
Deutscher Forschungszentren (HGF)

ISSN 0947-8620

urn:nbn:de:0005-069727

Abstract

In this report a state-of-the-art study was performed to investigate the operational conditions for in-core and ex-vessel materials in a future High Performance Light Water Reactor (HPLWR) and to evaluate the potential of existing structural materials for application in fuel elements, core structures and out-of-core components. In the conventional parts of such a novel plant the approved materials of supercritical fossil power plants (SCFPP) can be used for the given temperature ($\leq$ 600°C) and pressure ($\approx$ 250 bar). These are either ferritic/martensitic or austenitic stainless steels.

The design data for the in-core components are, however, very ambitious in comparison with conventional Light Water Reactors, especially regarding the coolant which is under high pressure ($\leq$ 250 bar) and will have a transition from sub- to supercritical state in the core, since the water temperature increases from 290 to 510°C outlet. The expected temperature in the cladding of the fuel elements can reach up to 650°C and the neutron exposure can accumulate up to $1.13 \cdot 10^{23}$ n/cm^2 or 60 displacements per atom (dpa) for an envisaged target of 70 GWd/t$_U$ burnup.

Taking these novel operational conditions into account an assessment of available material data was made. It is based on existing creep-rupture data, an extensive analysis of the corrosion in conventional steam power plants and the material behavior under irradiation. Compatibility between fuel and cladding materials is also considered. The potential of the different material groups available for in-core application, to be used as cladding materials of fuel elements, was further investigated by quantitative assumptions on the stress development in claddings and by a determination of the maximum achievable temperatures in dependence of cladding dimensions and the above mentioned operational conditions. More qualitative arguments on stress corrosion susceptibility are also included.

It was stated that for a maximum temperature of 650°C from a standpoint of creep-rupture strength and corrosion resistance not only Ni-alloys but also austenitic stainless steels would fulfill the requirements for application as cladding materials. Taking into account specific items like the neutron absorption, the sensitivity to irradiation-induced helium embrittlement and stress corrosion cracking, it was finally concluded that the austenitic stainless steels are the better choice.

The assessment has also shown that the most uncertain areas in the present analysis are the corrosion behavior under supercritical water conditions, including the effects of water chemistry/radiolysis, and the influence of a high stress state on stress corrosion and deformation mechanisms which govern the creep-rupture and creep buckling properties under irradiation. Future R&D activities should, therefore, concentrate on these open questions.

Zusammenfassung

Materialauswahl für in-case und out-of-case Werkstoffe eines zukünftigen HPLWR

Im Rahmen des HPLWR-Projekts (High Performance Light Water Reactor) wurde eine “state-of-the-art” Studie mit dem Ziel durchgeführt, die Betriebsbedingungen für sogenannte in-core bzw. ex-vessel Werkstoffe zu beschreiben sowie das Potential für existierende Strukturwerkstoffe für Brennelemente, Kernstrukturen und out-of-core-Komponenten abzuschätzen. Im konventionellen Bereich eines HPLWR können bewährte Werkstoffe aus fossilen überkritischen Kraftwerken bei $T \leq 600°C$ und Drücken von ca. 250 bar eingesetzt werden. Dies sind im wesentlichen ferritisch-martensitische und austenitische Stähle. Die Design-Anforderungen an die Kernkomponenten eines HPLWR sind im Vergleich zu normalen Leichtwasserreaktoren deutlich anspruchsvoller, da das Kühlmedium bei wesentlich höheren Temperaturen bzw. Drücken betrieben wird und im Kern des Reaktors ein Übergang von unterkritisch zu überkritisch, mit all den damit verbundenen Änderungen physikalischer Eigenschaften des Wassers, erfolgt. Die erwartete Oberflächentemperatur des Brennstabs kann 650°C bei einer Neutronenbelastung von bis zu $1.13 \cdot 10^{23}$ n/cm^2 oder 60 dpa und einem Abbrand von 70 GWd/t_U erreichen. Unter Berücksichtigung dieser Randbedingungen wurde eine Abschätzung des Materialverhaltens, basierend auf creep-rupture- sowie Korrosionsdaten aus konventionellen Kraftwerken und dem Materialverhalten unter Bestrahlung, durchgeführt. Weiterhin wurde auch die Wechselwirkung zwischen Brennstoff und Brennstabhülle berücksichtigt. Als ein wesentliches Ergebnis der Studie kann festgehalten werden, dass bei Temperaturen bis ca. 650°C aus Sicht der Kriechdaten, neben den bekannten Nickelbasislegierungen auch hochlegierte Edelstähle die Anforderungen erfüllen würden. Berücksichtigt man allerdings zusätzlich Daten wie die Neutronenabsorption, die Empfindlichkeit gegenüber einer He-Versprödung bzw. einer Spannungsrisskorrosion, so stellen die austenitischen Stähle letztlich die bessere Wahl dar. Die Studie hat aber auch aufgezeigt, dass nach wie vor große Lücken im Bereich der Wasserchemie, der Radiolyse, dem Einfluss von hohen mechanischen Spannungen bzw. Deformationsprozessen auf das Kriech- bzw. Kriechbeulverhalten, existieren. Die zukünftigen FuE-Arbeiten müssen dem Rechnung tragen.

TABLE OF CONTENTS: Page

1. Objectives of the study

Perform a state-of-the-art study that will guide in-core and out-of-core materials selection for the HPLWR.

Description of work

Evaluation of existing materials for fuel elements, core structures and piping and other relevant components based on assumed boundary conditions for a thermal HPLWR, and preliminary selection of appropriate candidate materials; Identification of potential future experiments.

Review of the effects of fluid radiolysis and power plant water chemistry on candidate HPLWR materials.

Activities

The activities of Work Package IV-Materials and Corrosion-started in September 2000. In the first year of this project study the work was concentrated on an overview of available materials, a description of their advantages and disadvantages, the compilation of most important creep-rupture data and an analysis of the corrosion behavior in conventional steam power plants. A first estimate of the temperature limits and dimensional design of fuel claddings, based on creep-rupture and corrosion data under assumed fuel pin operational conditions was elaborated. The results of the Working Group IV were summarized in the HPLWR Annual Technical Report from September 2001 [1].

In the second year this assessment was refined by a more quantitative description of the radiation damage parameters, effects of irradiation on material properties and an analysis of water chemistry and corrosion potential in conventional power plants and light water reactors, including the effects of irradiation-induced radiolysis. The potential of the different material groups to be used as cladding material of fuel elements was further investigated by more quantitative assumptions on the primary pressure development, the kinetics of uniform outer corrosion and the compatibility with the fuel as function of the time/burnup. Finally proposals were made for most important future work in a key technology phase of an HPLWR project.

Initially this Report was planned to be issued in early 2002. But taking into account that during the conceptual evolution of the HPLWR project new questions like the water chemistry of the system or the compatibility of the fuel with structural materials were raised to the Working Group IV, and that an extended evaluation of the potential of materials to be used as cladding materials for fuel elements were made, the study was completed with the final HPLWR Project Meeting in July 2002.

2. General selection criteria and operational conditions for in-core and ex-vessel components

The appropriate selection of materials for different components of a future HPLWR requires numerous materials data and a clear definition of the envisaged operational conditions. With such input an assessment of available material groups and a survey of the potential for the different alternatives can be provided.

2.1 General criteria and necessary data for material selection

The selection of appropriate structural materials for in-core and ex-vessel components requires the knowledge of conventional mechanical properties like tensile, creep, fatigue and fracture toughness data as well as information on the corrosion behavior under the existing operational conditions. For in-core application the material behavior under irradiation is a further, eventually limiting selection criterion. This includes nuclear data like integral cross sections for neutron absorption, which influence the neutron economy, and detailed knowledge about important transmutation reactions, which determine the neutron-induced radioactivity level, nuclear afterheat and the radiotoxic inventory of materials. Of great relevance is the material behavior under neutron irradiation which can affect the mechanical properties by leading to new phenomena of embrittlement, radiation hardening, irradiation creep, swelling and dimensional as well as structural instabilities of components. Also, for the special application as fuel cladding material, the compatibility with fuel material and possible effects of irradiation on corrosion has to be taken into account.

Dependent on the application as ex-core or in-vessel material a part or all of this information has to be available for a thorough assessment. Taking into account the limited budget and scope of the project, a complete material analysis is far beyond the scope of the present HPLWR study.

2.2 Operational conditions for in-core and ex-vessel materials

2.2.1 Reference and extended design data

The work was started by adopting Oka´s HPLWR design data [2] as reference for in-core fuel element assemblies and adding Bittermann´s [3] design recommendations for the Reactor Pressure Vessel (RPV). For the ex-vessel components the presently used parameters for mature supercritical conventional power plants were taken from [4]. Table 1 gives a compilation of these initial “Reference Design Data”. In two Working Group IV meetings [5-6] the data for in-core application were modified by extending the maximum burnup of fuel elements to 70 GWd/t_U, which corresponds to a lifetime of about 45,000 hours and to allow MOX fuels for an enrichment of about 5%. Also, a higher pin pre-pressurization (8 MPa) and a linear increase of the inner pressure by fission gas release with time ($2.2 \cdot 10^{-4}$ MPa/h) were adopted. Table 1 also contains coolant pressure and temperature data to be expected in the different components and requirements for the expected lifetime of the RPV and ex-core components. Potential materials considered for application in different components are also added. The initial estimates in Oka´s study on cladding dimensions and maximum achievable surface temperatures are also given for information, though our study leads to partially different results as discussed below.

Table 1: HPLWR "Reference" Design Data for in-core [2], RPV [3] and ex-core components [4] and modifications in [5, 6]

In core data	
Coolant Coolant pressure [MPa] Coolant inlet/outlet temperature [°C]	 25 280/508
Fuel/Enrichment Fuel/Enrichment, revised [5]	UO_2/≤5% MOX/ to be determined
Burnup [GWd/t_U]/ lifetime [hours] Burnup [GWd/t_U]/ lifetime, revised [5, 6]	45/30,000 70/45,000
Neutron flux [n/cm^2·s] /fluence [n/cm^2]	$5 \cdot 10^{14}$/ $8 \cdot 10^{22}$
Cladding outer-diameter/thickness [mm] [2] Cladding max. surface temperature [°C] [2]	8/0.4 620 for Ni alloys 450 for stainless steels
Pin pre-pressurization [MPa]	≤ 4 [2]; Revised [5, 6]: ≤ 8
Potential core structure and cladding materials Austenitic stainless steels Ferritic/martensitic steels Ni-based alloys	 1.4550, 316L(N), 1.4970 1.4914, FV 448, EM10 PE 16, Inconel 625, Inconel 718
Reactor pressure vessel	
Coolant pressure [MPa]	25-27.5
Temperature [°C]	350
Lifetime [years]	60
Materials	Ferritic steels (20 MnMoNi 5 5)
Ex-core data	
Life steam pressure [MPa] Life steam/reheat temperature [°C]	25-27.5 540/560
Lifetime [h]	200,000
Materials Ferritic/martensitic steels Austenitic stainless steels	 X20 CrMoV12 1, P91, E911, P92 (NF616), P122 (HCM12A) 1.4910, TP347HFG, Super304, NF709, Incoloy 800 HAT

2.2.2 Irradiation conditions

Neutronics and radiation damage parameters

Oka´s reference design has been evaluated with respect to the neutronic data by G. Rimpault and E. Testa [7]. For the assessment of possible material problems the neutron flux and spectrum are of great importance since from them typical material damage parameters like the number of displacements per atom (dpa), neutronic absorption and the generation of important transmutation products like helium and hydrogen by inelastic reactions with neutrons can be calculated. Also the expected activation and nuclear afterheat of each material group can be determined.

According to Rimpault and Testa the total average and maximum neutron flux data are 3.2 and $7.0 \cdot 10^{14}$ n/cm^2·s, and the fluence levels accumulated during 45,000 h of irradiation are 5.2 and $11.3 \cdot 10^{22}$ n/cm^2, respectively. The fraction of neutrons with an energy equal or larger than 1 MeV is in the range of 23 %. Calculated displacement damage rates for Fe are: $2.2 \cdot 10^{-7}$ on average and $4.9 \cdot 10^{-7}$ dpa/s in the maximum position. Tanskanen´s and Wasastjerna´s [8] results of damage rates calculated with MCNP by using cross sections from IRDF-90 are about 23 % lower for Fe, with 1.7 and $3.8 \cdot 10^{-7}$ dpa/s. They also investigated the displacement rate for Ni which is $4.2 \cdot 10^{-7}$ dpa/s in maximum position. It is, however, recommended that for a first estimate the data for Fe can reasonably well be adopted also for important alloying elements of steels and Ni-based alloys. This leads then to an average number of 27.6 dpa and max. 61.8 dpa after an exposure of 45,000 h, if the damage rate data of Tanskanen are taken. As will be discussed under Chapter 4 this is already a very high displacement damage, where typical high fluence radiation damage phenomena like swelling and creep are of great importance for the dimensional stability of fuel elements and core structures.

The variation of k_{eff} with material has also been investigated by Rimpault [7] and Tanskanen [8]. Rimpault gives for a typical stainless steel (AISI 316) a k_{eff} value of 1.237 and for Inconel 625, a typical Ni alloy, 1.185. Tanskanen reports 1.148 for type 1.4970 steel and for Inconel 718 a value of 1.0975. Though both data differ somewhat one can say that the contribution of the Inconel to the total neutron absorption is in the range of 14 % and that of the austenitic steels about 10 %. By using stainless steels the necessary average enrichment to achieve a burnup of 70,000 GWd/t_U can be reduced by 0.9 % when compared with a Ni-alloy as core structural and cladding material.

Helium generation

For the high temperature embrittlement, which is caused by the formation of helium via inelastic n,α-reactions, calculations have also been made by Tanskanen [8] for the alloys 1.4970 and Inconel 718 as typical representatives of austenitic steels and Ni-alloys. The formation of helium in atomic parts per million (appm) in dependence of irradiation time is shown for both materials used as cladding materials in Fig. 1. Two major reactions contribute the essential part in a mostly thermal neutron spectrum, namely the $^{10}B(n,\alpha)Li^7$ and the $^{58}Ni(n,\gamma)^{59}Ni(n,\alpha)^{56}Fe$-double reaction. The first reaction dominates at the initial phase and the obvious saturation of helium production in 1.4970 at a level of around 85 appm He is caused by the complete

burn-out of 80 appm ^{10}B isotope, which is about 20 % of the natural boron content (80 wppm!) in this alloy. Inconel 718 also contains boron on the level of 60 wppm, which is burned out at nearly the same rate as for the austenitic steel, so that about 60 appm helium are generated in Inconel 718 via the B(n,α)Li reaction.

The much higher Ni in Inconel 718 content produces via the Ni double-reaction in this fluence range about $2.5 \cdot 10^{-7}$ appm He/s compared with about $7 \cdot 10^{-8}$ appm He/s in the alloy 1.4970, about 4 times more helium. This latter reaction dominates at higher fluence levels or longer exposures and discriminates both curves, which is especially important, if the materials are not periodically replaced like in the case of fuel elements, but remain in the core as core structures over the whole reactor life of about 40 or 60 full power years.

Boron is an important alloying element in austenitic steels as well as in Ni-alloys, because it improves the high temperature creep strength. A reduction of the He production via the B(n,α)-reaction under irradiation is possible, by using instead of natural boron isotopically clean B-11, which has a very low (n,α) cross section. The separation of both boron isotopes is technically possible and widely used for the fabrication of absorber steels.

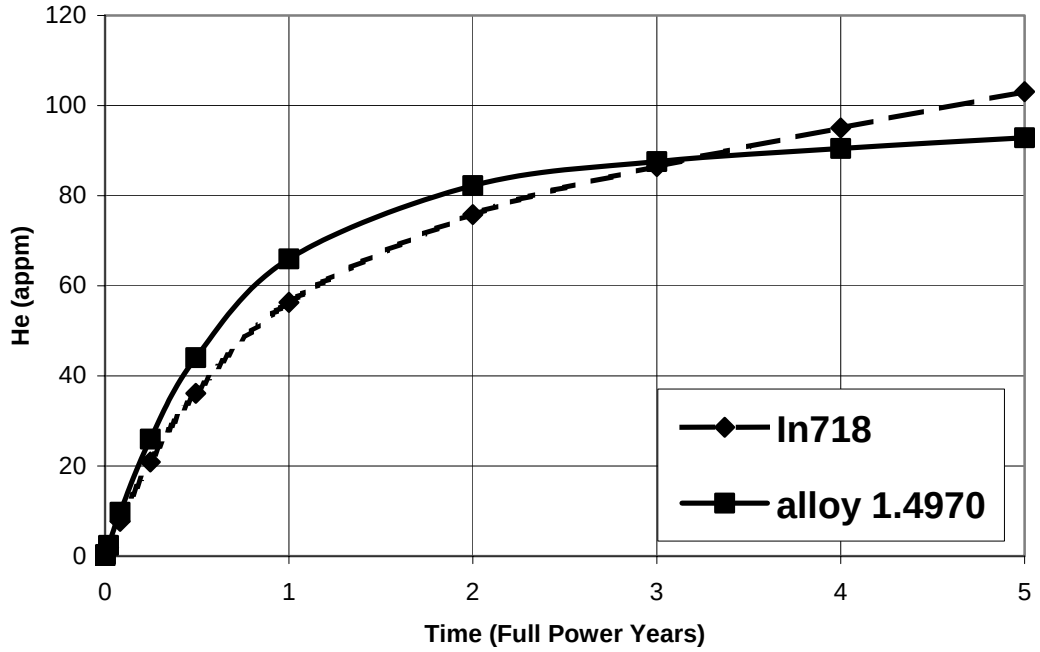

Fig. 1: Helium production in steel 1.4970 and Inconel 718 during irradiation in HPLWR [8]

2.2.3 Water chemistry and radiolysis

Introduction

Feedwater for BWR, PWR and once-through cycles of future HPLWR's must meet specific quality requirements to ensure a safe and economic operation. If the water/steam is circulated in a closed cycle (PWR), the quality of circulating water and steam must be suitable for all components in the water/steam cycle and is therefore dependent on the material concept for the whole plant. This leads to more strict specifications than the individual plant components would demand.

The purpose of a controlled water chemistry in a water/steam cycle of a water-cooled nuclear reactor is to minimize the corrosion of structural materials and hence the mass transport of corrosion products within the water/steam cycle. With this measure deposits or crud within the water/steam cycle should be reduced to a minimum. Besides the basic principles of power plant chemistry to reach the objectives, like using demineralized water, limiting the ingress of impurities to the water/steam cycle and controlling the pH-value, the different reactor concepts require a specially adapted water chemistry to ensure a safe operation [9, 10].

Formation of protective oxide layers

The oxidation is controlled by the steel composition, as reviewed earlier in HPLWR-WP IV reports, and by the temperature. The corrosion attack of water/steam fluid is leading to the formation of iron oxides. The corrosion rate is limited by the formation of a superficial protective uniform oxide layer. The only natural oxide which can exist in direct contact is magnetite. The basic chemical reaction between steel and water leads to iron dissolution within several reaction stages: Redox reaction from Fe(II) to Fe(III) and condensation stages (Schikorr reaction), leading to the formation of magnetite. Based on these interactions, water/steam cycles in power plants can be divided into two areas:

- The temperature range up to 200°C. Schikorr reaction assures that the steel surface in contact with water remains active in respect to iron dissolution and

- The hot water range above 200°C, where a magnetite protective layer forms spontaneously.

Mass transport of corrosion products

Due to the decrease of solubility with temperature of iron in hot water, magnetite tends to precipitate from aqueous solutions above 200°C. This can lead to dramatic reductions in cross-sections and to a distinct change of heat-transfer conditions in steam generating tubing.

Other undissolved corrosion products will be carried along the water/steam cycle and can be deposited on thermally high stressed tube walls of boilers. This can have a detrimental effect on the stability of such components. On the one hand, the formation of thermally insulating layers can lead to an increase in temperature and thereby to a reduction in mechanical strength due to overheating. On the other hand,

under deposits, dissolved electrolytes can be enriched, hence initiating a chemical attack on both, the metallic tube material and the protective layer.

Impurities

Impurities in water/steam have to be strictly controlled because they can cause corrosion and deposits on components of a water/steam cycle (Table 2). By comparing the values from Garzarolli [11] with the levels for “normal operation condition”, given in the 1996 revision of VGB_R 401 J [10] and the PWR data in [9] it is obvious, that the VGB-values for BWR’s are much stricter, with narrower ranges of variation (definition of action levels 1-3, too), especially for the feedwater, compared to the reactor water. Hence, a preference for the newer “VGB-data” is concluded.

In view of the inhibiting effect of oxygen on steel in demineralized water/steam, special care has to be taken on the concentration by means of different *“oxygen chemistries”*. However, if the specified conductivity for demineralized water (< 0.2 µS/cm) is exceeded due to system leakages, it is necessary to stay at a lower oxygen level of about 0.02 mg/l for a short period of time.

Iron and copper concentrations in the water/steam are an indicator of the efficiency of conditioning. Their values give information about the corrosion/deposition processes in the water/steam cycle, respectively in the boiler and turbine. Both levels should therefore be maintained in the wppb-range.

Silica concentrations in once-through boilers may not exceed certain values due to the specification for turbine operation. When operating with fully demineralized water, the silica content will be far below the specified level. Some problems can arise when colloidal silica is present in the feed water and was thereby not retained during the water treatment processes.

Table 2: Water chemistry in BWR’s and PWR’s (normal condition) after Garzarolli et al. [11] and VGB [9]

Reactor type	**pH**	**Conductivity µS/cm**	**Li wppm**	**B wppm**	**H wppm**	**O wppb**	**Fe wppb**	**Cu wppb**	**Cl wppm**	**Solids wppb**
BWR	5.5	0.1-0.3	-	-	0.025	200	0.5-10	0.1-1		1-10
PWR	6.9-7.3	*****	1-2	0-1500	2-4	<1	1-10	-		1-10
PWR, VGB [9]	6.9-7.4	<1*****	0.2-2.2	0-2500	1-4	<5	<10	-	<0.2	

**: Depending on B (and Li) concentration*

Water chemistry in BWR’s, PWR’s and HPLWR’s

BWR’s have an open cycle, operate at system pressures of 70 bars at typical temperatures of 285°C and form steam in the core. The water is separated from the steam within the pressure vessel and the steam is taken directly to the turbine and to the condenser. Due to the corrosion of structural components, about 10-100 kg of

crud is deposited on the fuel elements per full power year. These deposits contain mainly iron and in some plants copper, too.

Another important aspect of BWR's is the water radiolysis in the core, which leads to oxygen concentrations of 200 to 300 wppb in the water and 20 to 30 wppm in the steam. The corrosion potential at an oxygen level of 200 wppb lies in the range of -0.1 and 0 V (SHE). In some BWR's, hydrogen is added to reduce the oxygen content in the feedwater (HWC). However, the radiolytic oxygen in the core cannot be suppressed by such hydrogen addition. Under such conditions, the hydrogen becomes stripped off from the water to the steam phase. The normal water chemistry is called NWC, whereas the hydrogen modified one is termed HWC.

PWR's have a closed cycle. The water is pressurized up to about 150 bars and is circulating through a steam generator and back to the core. The core entrance temperatures range from 280 to 295°C and reach values between 300 to 340°C at the exit of the core. The water chemistry is controlled by additives (see Table 2). Boric acid is added for controlling the reactivity and hydrogen for suppressing the formation of radiolytic oxygen. Numerical considerations have shown, that hydrogen concentrations above 0.5 wppm are enough to control the radiolytic oxygen. As a consequence, hydrogen is kept usually between 2 to 4 wppm. To maintain the pH at an appropriate level, lithium as LiOH, is added in the wppm-range.

No data for water chemistry are available for **HPLWR's** because this reactor type is at a conceptual level at the moment. Nevertheless, experiences from BWR, PWR and Supercritical Fossil Power Plants (SCFPP) can be used when discussing the special conditions of water chemistry for HPLWR's. Due to the fact that in a HPLWR, the coolant water remains in a single-phase condition (subcritical water $\rightarrow$ supercritical water) along the whole once-through cycle, a control of the oxygen by adding of hydrogen, like in PWR's or in BWR's, seems to be very likely. Based on the current information it is concluded, that the water chemistry of conventional SCFPP's and of PWR's or BWR's could be combined to define specific conditions for a HPLWR (Tables 2, 3).

Table 3: Main water chemistry characteristics of fossil fuel power generating units [12, 13]. The data is valid for the feedwater region and specified for turbines with inlet pressure of 13.6 MPa/VGB and 19.7 MPa/EPRI and with a hydrazine-ammonia (N_2H_4/NH_3) water chemistry in both.

Specification	pH	Conductivity µS/cm	Fe total wppb	Cu total wppb	Na wppm	Silica wppm	O wppb
VGB [12]	9 - 10	0.1	10	1	2	5	<100
EPRI [13]	9.2 - 9.6	<0.2					

Comparing between Tables 2 and 3, it can be stated that with regard to water chemistry a combination of the boiler cycle of conventional power plants and the in-core reactor cycle of an integrated once-through system could be adapted to the HPLWR. A limitation may be the different pH values in both cycles. The need for the basic hydrazine-ammonia chemistry for the ex-vessel components should be studied further.

Radiolysis

Regarding the radiolysis in supercritical cores, no data are available. Nevertheless, some statements concerning the expected conditions can be made:

Basic considerations

The concentration of radiolytic water decomposition products according to the following equation

$$2H_2O \overset{(n,\alpha,\beta,\gamma,fp)}{\Leftrightarrow} 2H_2 + O_2 \quad (1)$$

with typical radiolysis products of e^-_{aq}, H, H_2, OH, H_2O_2,O_2^-, HO_2, O_2, H^+ and OH^- is depending on:

- the reactor power, irradiation dose, particle and energy absorption in the core
- the coolant temperature, pressure and flow rate
- the chemical composition of the coolant in respect to additives (gases, solids) and impurities

Regarding the chemistry, e^-_{aq}, H and H_2 are attributed to a reducing character of the coolant water, whereas H_2O_2 and O_2 are known as oxidizing species. With pure water in a closed single phase system, they generally balance out so that there is no overall oxidizing or reducing effect [14].

Outlook on radiolysis in a supercritical HPLWR-system

The maximum content of radiolytic water decomposition products will not exceed the normal values in a BWR (200-300 wppb O_2)

Compared to a BWR

- The higher system pressure will minimize water radiolysis according to Eq. 1 by shifting the equilibrium to the water-side
- The higher system temperature will favor the recombination of activated radiolytic products (radicals)
- The addition of hydrogen to the system (like in a PWR) will reduce the radiolytic oxygen production significantly.

The potential influence on oxide scale composition (stoichiometry), besides oxide defect structure and transport mechanisms during corrosion seems to be negligible.

In consequence, it can be expected that under HPLWR conditions uniform and local corrosion will not be accelerated by water radiolysis.

3. Out-of-core materials

The selection of appropriate structural materials for ex-vessel components can be based on the data and experience developed for conventional combustion plants operating in supercritical (SC) regime. These data are today available from the material development for super heater tubes, hot sections and turbine materials and research projects covering also service properties, creep and oxidation. Open data about the behavior of these steels in operating conditions are still limited, mainly due to the early stage and small amount of new SC-plants in Europe.

Due to the fact that the present steels have a rather good creep strength within the aimed HPLWR temperature range (out-of-core maximum 600°C) the crucial point for material selection in future HPLWR's will be the corrosion behavior under supercritical service conditions. The oxidation may be the life-limiting factor in thin wall tubes.

The corrosion behavior study includes the evaluation of metal loss due to oxidation as well as the influence of stress on the corrosion behavior in such systems. At present the modern supercritical power plants are contributing to our operational experience; the use of modern material is evaluated in respect to long-term corrosion from conventional steam boilers.

3.1 Selection of materials

A literature review on potential steels suitable or used for ex-core application in different components under supercritical (SC) and ultra supercritical (USC) conditions was performed [15-19]. Based on this survey a listing of commercial modern SC fossil fuel power plant steels was made for out-of-core materials in Table 4. The list of materials includes the groups of 2.25 Cr- and 9-12CrMoWV steels in non-stabilized or Nb-stabilized versions and the large family of austenitic stainless steels, starting with the classical 18Cr-9Ni versions and including the high Cr-Ni alloys of type 20-25Cr 20-25Ni, used predominantly in superheaters. The mechanical data of these alloys are well known in the interesting temperature range of 550 to 650°C and the main efforts have been in the field of corrosion. Moreover, the oxidation analysis has been extended to the Ni-alloy Inconel 625, which, as a representative of Ni-based alloys, has the potential for in-core application.

Table 4: Materials for key components in USC power plants
[Blum, 1998; Husemann, 1999]

Component/ Material	Composition	Max. steam temperature for p = 325 bar
Furnace panels		
HCM2S	**0.01C-2.25Cr-0.3Mo-1.6W-V-Nb-N-B**	**625**
7CrMoTiB1010	**0.07C-2.4Cr-iMo-V-Ti-N-B**	**625**
HCM12	**0.1C-12Cr-1Mo-1W-V-Nb-N**	**650**
Super heaters		
TP347HFG	**18Cr-10Ni-1Nb**	**~620**
Super 304H	**18Cr-9Ni-0.4Nb-Cu-N**	**~625**
NF709	**20Cr-25Ni-1.5Mo-0.25Nb-0.05Ti-N**	**~630**
Esshete 1250	**0.016/0.15C-14/16Cr-9/11Ni-0.8/ 1.2Mo-0.72/1.25Nb-N-B**	**~620**
HR3C	**25Cr-20Ni-0.4Nb-N**	**~630**
Thick section boiler comp.		
NF616	**0.1C-9Cr-0.5Mo-1.8W-V-Nb-N-B**	**610**
HCM12A	**0.1C-11Cr-0.5Mo-1.8W-1Cu-V-Nb-N-B**	**610**
Turbine rotors		
COST E/F	**0.12C-10Cr-1Mo/1,5Mo-1W/0W-V-Nb-N**	**610**
COST B	**0.17C-9.5Cr-1.5Mo-0.01B-V-Nb-N**	**625**
HR1200	**0.09C-11Cr-0.2Mo-2.7W-2.5Co-V-Nb-N-B**	**630-650**

3.2 General corrosion behavior under sub- and supercritical water conditions

The corrosion of structural materials in supercritical water has been extensively investigated in high-oxygenated water in the frame of research for the Supercritical Water Oxidation Process (SCWO) [20, 21]. Although the conditions in a future HPLWR are very different regarding the contents of oxygen and other impurities, some principal issues may be of general validity.

For materials like steels and nickel-based alloys the principal corrosion rates as a function of pressure and temperature are shown in Fig. 2.

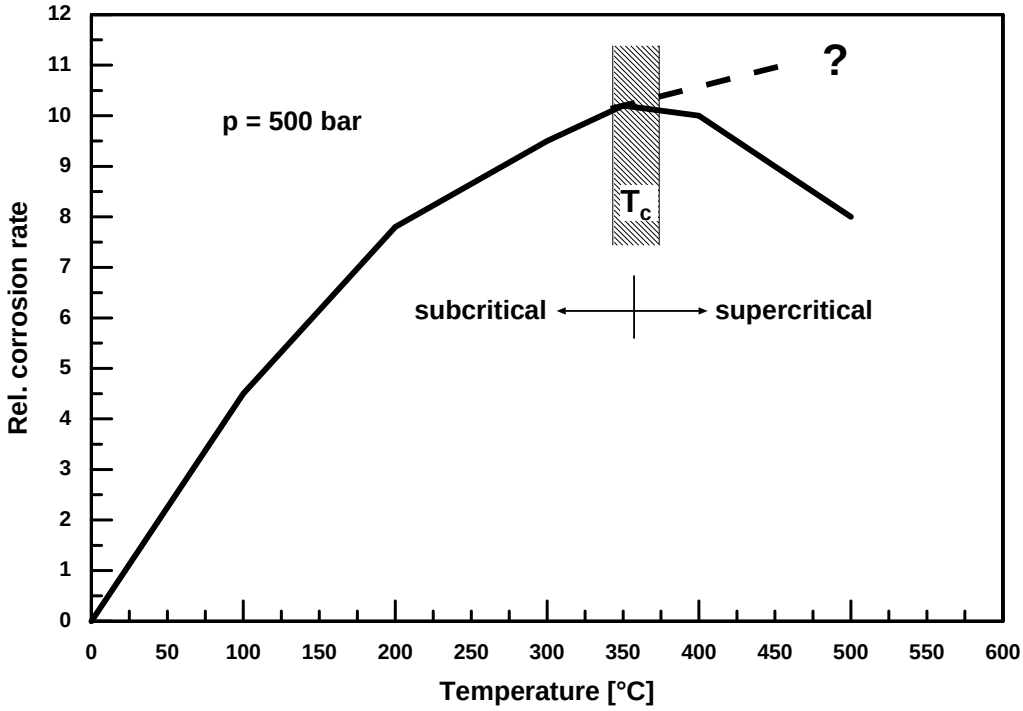

Fig. 2: Relative corrosion rate of alloys in high-oxygen/chloride water at 500 bars (oxygen is in great excess) after [22]

It is obvious, that the corrosion rate has a maximum around the critical temperature and decreases in the supercritical range. The maximum of the curve is explained as a result of a) the increase of the corrosion rate with temperature (Arrhenius-type) and b) the decrease of the dissociation constant and the density of water with temperature (c_{H+} becomes lower). Whether the maximum corrosion rate around the critical point of water (ca. 374°C) is typical for very low-oxygen water, or the increase of the corrosion rate far into the supercritical range as indicated by the dashed line in Fig. 2, is true, has to be validated by further investigations. For a conservative assessment of the corrosion rate, it is therefore agreed to rely on existing sub- and supercritical data.

Longton [23] presented in a review of seven publications of 1954-1965 a report in which he compared the results of corrosion experiments in steam at superheat temperatures (427-816°C) and subcritical, near critical and supercritical pressures (70-350 bar). He pointed out, that the measured corrosion rates differ not remarkably when those of subcritical (70 bar) and supercritical (350 bar) steam exposures are being compared. If differences exist, they lie in the scatter band due to other parameters, like preparation of metal surface, corrosion test procedure, specimen geometry, steam composition, etc.. Regarding the latter parameter, only occasionally oxygen and/or hydrogen were added for simulation of radiolysis in the wppm range.

Experimental data of Boyd et al. [24] on the corrosion of different materials in low-oxygen, deionized distilled water (see Table 5) supported the corrosion behavior, expressed by the dashed line in Fig. 2. The rate constants were calculated using the formula

$$w = k \cdot t \qquad (2)$$

where w is the weight gain in mg/dm^2, t is the exposure time in days and k is the linear rate constant in mg/dm^2·d (estimated for durations of ca. 3,500 h).

Table 5: Linear rate constant k in supercritical water at 345 bar after [24]

Materials	***k* (427°C) mg/dm^2·d**	***k* (538°C) mg/dm^2·d**	***k* (732°C) mg/dm^2·d**
SS 410	0.05	0.1	1.2
AMS 5616	0.2	0.3	0.39
Armco 17-4 PH	0.1	-	0.3
Armco 17-7 PH	0.033	0.067	0.48
SS 302	0.1	0.66	4.7
SS 347	0.01	0.26	9.83
SS 309	0.073	0.29	0.83
SS 310	0.11	0.17	0.87
Allegheny A-286	0.07	0.18	9.3
Inconel X	0.011	0.97	6.7
Hastelloy F	0.011	0.22	0.39
Hastelloy X	0.024	0.31	1.8

At the highest test temperature of 732°C, only the Armco-type 17-4 and 17-7 steels and the nickel-based Hastelloy F showed an acceptable corrosion behavior with corrosion (oxidation) rates of about 3-6 µm/a. The surfaces of the resistant alloys were covered with an adherent oxide coating, although most of the attack was localized and selective. At the lower temperature of 538°C, most of the alloys revealed only slight uniform general attack with a rate of less than 1 µm/a for the resistant Armco-type steels. At 427°C, an excellent appearance of all samples was found due to the coating by good adhering oxide films.

In contrast to the results at constant supercritical test conditions in steam, a different corrosion behavior was described under constant supercritical pressure when temperature transients were applied [25-27]. These conditions caused -during exposure of highly corrosion resistant alloys to an aqueous, slightly contaminated medium- heavy local corrosion attack. It was measured in-situ and by post-test evaluation by means of electrochemical noise signals, sonography and metallography.

By measuring the electrochemical noise amplitude, Liu et al. [25] exposed various metal surfaces to an aqueous supercritical solution containing oxygen (saturated) and 0.1M HCl. When passing through the temperature range of transition to supercriticality (critical point), a remarkable increase of corrosion under “boundary conditions” was observed. At higher temperatures, the extent of uniform corrosion drastically diminished. These phenomena were explained by a sudden change of corrosion mechanism from an electrochemical local one to a chemical uniform one, going along with a rapid decrease of density and solubility, i.e. concentration of aggressive species (HCl, O_2) in solution, with increasing temperature above the critical point.

A maximum corrosive local attack was observed by Boukis et al. [26] within an externally heated/internally steam exposed tube specimen. The flowing, slightly chloride and oxygen contaminated steam at supercritical pressure passed through the heated section of the tubing and experienced the transition to and from supercritical conditions twice. On both tube sides, i.e. at the entrance and at the exit, heavy local corrosion was observed while in the middle low uniform attack occurred.

These observations are confirmed by Modell [27] who exposed a corrosion resistant test wire in full length into a tubular reactor, filled with waste sludge and mixed with oxygen which reacted at supercritical conditions (600°C, 250 bar) for total waste destruction. In the temperature transient tube lengths, heavy corrosion attack and finally fractures of the wire were found at the entrance and exit as well.

Comparing the corrosion rate in low-oxygen/chloride water from [24] with the corrosion in high oxygen/chloride water under SCWO conditions [20-22, 25-27], a different behavior is obvious, as shown by the maximum of the rate (full line) in Fig. 2. Further experiments have to prove, if the general or uniform corrosion of potential alloys like ferritic and austenitic steels is increasing or decreasing when changing from sub- to supercritical water under HPLWR-conditions.

Corrosion under in-pile superheat conditions

Within the General Electric EVESR-Superheat Reactor Programme, the so-called Mark II annular superheat fuel and the Mark III rod cluster superheat fuel were tested in BWR-typical, subcritical steam of 70 bar with 20 wppm O_2 and 2.5 wppm H_2 [28-29].

Annular superheat fuel

Exposure of four cladding materials

- SS 304 (commercial grade, vac. melted)
- SS 310 (vac. melted)
- Incoloy 800
- Inconel 600

The exposure of 308 Mark II annular rods, of which only 3 rods failed, was performed as follows:

- Time at power: 7 254 – 14 030 h
- Spec. peak cladding temperature: 700°C
- Max. heat flux (without skew): 37 - 51 W/cm²
- No. of thermal cycles: 124 – 152
- Peak burnup of leading rods: 4 000 – 7 000 MWd/t_U

Results concerning corrosion

All four cladding materials exhibited a high resistance against corrosive attack of superheated steam under heat-transfer and irradiation. The depth of the affected wall thickness did not exceed 50 µm. The appearance and thickness of the oxide scales correlated with observations made in previous out-of-pile examinations. The formation of tightly adherent oxide scale on SS 304 of about 38 µm was double the

scale thickness as observed on the other 3 alloys. No evidence of intra- or transgranular SCC was found.

Rod cluster superheated fuel

Exposure of one cladding material

- Incoloy 800

The exposure of 4 seven-rod bundles Mark III superheat fuel, in which the cladding wall thickness of 200-500 µm was the principal variable, was performed as follows:

- Time at power: 6 777-10 292 h
- Peak steady state cladding temperature: ≤ 740°C
- Peak Heat flux: 94 W/cm²
- Peak burnup of leading: 9 300 MWd/t_U
- Peak integrated fast neutron flux: $6 \cdot 10^{20}$ n/cm² (> 1MeV)

Results concerning corrosion

General corrosion of Incoloy 800 was characterized in appearance and depth as equal to that observed out-of-pile in steam loops. The affected wall thickness, including local penetrations, did not exceed 25 µm.

3.3 Investigations on the corrosion behavior in steam of selected materials relevant for fossil fuel power plants

The oxidation kinetics has been studied for the uses in fossil fuel power plants (coal fired boilers) where SC-conditions have been adapted to enhance the efficiency in combustion of coal.

In this study the oxidation kinetics is needed when evaluating a) the loss of metal in tubes for stress calculations and b) the formation of oxide debris in the cycle. In the ex-vessel case the accuracy needed for the evaluation is the order of +/-10 - +/- 50 µm for the metal loss. However in the assessment of in-core fuel cladding oxidation the accuracy must reach +/-10 µm or better over the aimed 5 years (45,000 h) period.

A more detailed study of the oxidation kinetics of the materials in steam at 550 – 650°C was collected from the recent literature covering the main results of the finished COST 501 and started COST 522 actions as well as latest conference papers from VDI and other European and Japanese sources [30-33]. Examples of this survey and the collection of data and list of references are shown in Fig. 3. In this evaluation three ferritic/martensitic steels (f/m) and two austenitic stainless steels were included:

The F/M steels are:

- 2.25Cr1Mo, a classic F/M steel for reference

- P91, a 9%Cr steel, developed for SC super heaters with excellent creep properties

- HCM12A, a 12 % Cr steel with outstanding creep and oxidation resistance

The austenitic steels are:

- 1.4910, a fully austenitic 17-12 Cr-Ni-N stainless steel with a 2.5 % Mo addition
- TP347HFG, a Nb-stabilized fine grained 18-10 Cr-Ni steel with a 1 % Nb addition

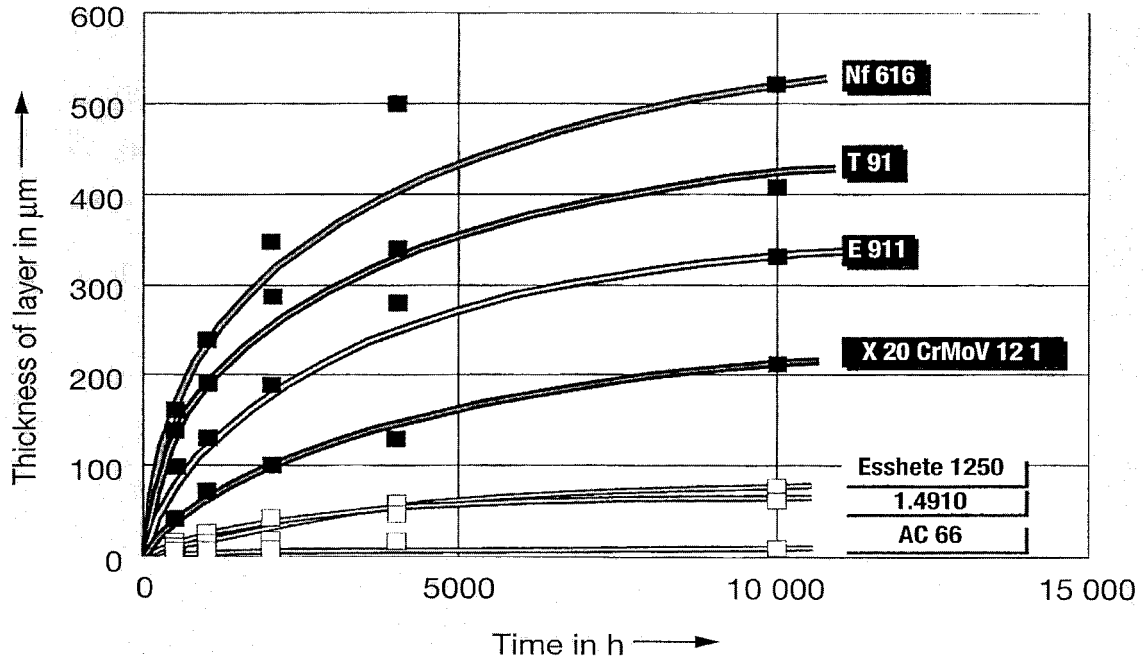

Fig. 3: Corrosion rates, oxide layer thickness versus time, of 9–12 % Cr f/m-steels X20 CrMoV 12 1, E911, T91 and NF616 and austenitic steels Esshete 1250, 1.4910 and AC66 at 630°C under steam. [Tolksdorf, 2000 in Ref. 32]

Moreover, the oxidation data of the Ni-alloy Inconel 625 alloy has been collected [34-36]. This alloy is also very relevant for in-core application.

The fact is that the corrosion measurements have not been uniformly standardized, which means that there is a wide variety of measurement and monitoring techniques for oxidation offering data in appropriate forms for specific purposes. Also in many cases there are data available only at certain conditions, e.g. at one temperature, that does not allow the processing of a general kinetic formula. Therefore, mixing of data from different authors may not yield accurate assessment. Based on the literature survey it was decided to use the data of Husemann [30] to process kinetic equations for the oxide layer growth of the selected steels, because this data set was found to be most consistent for this study. The intention is to correlate later on the data of other authors to the processed kinetic equations.

3.3.1 Oxidation kinetics of steels

The general oxidation is regarded to be the corrosion rate-controlling factor in dry steam environment for the selected steels. The oxidation growth kinetics is assumed to follow the parabolic growth that is valid for most of the oxidation processes. It is also possible to use a linear correlation, especially with short exposure times or when spalling off of the scale takes place. In this study first a stable parabolic oxide growth is evaluated and then a linear spallation factor is included in the kinetic formula.

The kinetic data for the f/m and austenitic steels have been extrapolated from parabolic rate constants, k_p, provided by Husemann [30] to cover the studied temperature range (T = 550–650°C) and the required life time (t = 45,000 h), using fitting algorithms by standard software (Origin 6.0).

The resulting kinetic equations for oxidation, the oxide layer thickness, as a function of time and temperature are presented in the form of an Arrhenius equation, Eq. 3, in which the first term corresponds to the parabolic oxide growth. The coefficients for this equation (A and B) are listed in Table 6 for the different steel types. The fact that the growth of the oxide layer is not stable needs also the spallation coefficient (sp) for the oxide to be taken into account in Eq. 3, where the second term corresponds to the linear time dependency. This term has recently been introduced by the COST 522 group (Knödler et al. [33]), Table 7.

Table 6: Oxide growth constants (in Eq. 3) for Arrhenius equation of selected alloys. The spallation coefficient at 650°C [mg/cm^{2}h] stems from [Knödler et al., Ref. 33]

Steel	A [µm/h$^{0.5}$]	B [K]
2.25CrMo1	1900400	-14402
P91	9278	-8114
HCM12A	79179	-10842
1.4910	83680	-10897
TP347HFG	63588	-11309

* data are available as graphs and tables (Origin 6.0)

Table 7: Oxide spallation coefficients at 650°C) [mg/cm^{2}h] from [Knödler et al., 2001]. The density of oxide is assumed to be 5 g/cm^3

Steel	Spallation coefficient 650°C [mg/cm^{2}h]	Spallation constant [µm/h]
2,25Cr1Mo	$4 * 10^{-3}$	$8 * 10^{-3}$
P91	$3 * 10^{-3}$	$6 * 10^{-3}$
HCM12A	$2 * 10^{-4}$	$<4 * 10^{-4}$
1.4910*	$< 10^{-4}$	$<2 * 10^{-4}$
TP347HFG*	$< 10^{-4}$	$<2 * 10^{-4}$

* estimated for the data according to Knödler

The spallation coefficient is assumed to be also a function of temperature and, therefore, based on the data of Knödler and the derived metal coefficients B, in this work, the temperature dependence of spallation is determined for the studied steels in Table 8. Here the normalizing is carried out using the temperature dependency of the parabolic growth at the actual temperature ($e^{B/T}$) to the B-value of Knödler et al. at 923 K ($e^{B/923}$) from Table 3. The corresponding loss of metal is achieved by multiplying these values with 0.5.

The final formula for the oxide growth is in Eq. 3:

$$D_{ox} = A\, e^{B/T}\, t^{1/2} + sp*t \qquad (3)$$

- *D_{ox} = oxide thickness [µm]*
- *t = time [h]*
- *T = temperature [K]*
- *A = parabolic constant [$\mu m/h^{0.5}$]*
- *B = E/R, where E = activation energy & R = gas constant, [K]*
-

Corresponding metal loss can be calculated from Eq. 4:

$$D_{Me} = 0.5*D_{ox} \qquad (4)$$

Table 8: Spallation coefficients at different temperatures for the studied steels, the spallation coefficient at 650°C is from Knödler et al. [33] and the normalizing factor for the SP values at 600 and 550°C used is $(e^{B/T})/(e^{B/923})$, from Table 7.

Steel	**SP at 650°C [µm/h]**	**SP at 600°C [µm/h]**	**SP at 550°C [µm/h]**
2.25Cr1Mo*	0.008	0.0033	0.0012
P91*	0.006	0.0025	0.0009
HCM12A*	0.0004	0.00016	0.00006
1.4910**	0.0002	0.00008	0.00003
TP347HFG**	0.0002	0.00008	0.00003
* from Knödler & al. 2001			
** The study of Knödler et al. does not cover the austenitic alloys; the information is personal from Knödler for these alloys.			

The growth can be used directly to assess the loss of metallic material during operation as a function of time and temperature, with the correlation of oxide density to metal density assumed to be 0.5 valid for ferrous materials. The oxidation kinetics of the potential steels is shown in Figs. 4-8. The spallation effect is almost negligible in these steels except for the 2.25 % Cr steel. Therefore, in Figs. 4-8 only the stable oxide growth is described.

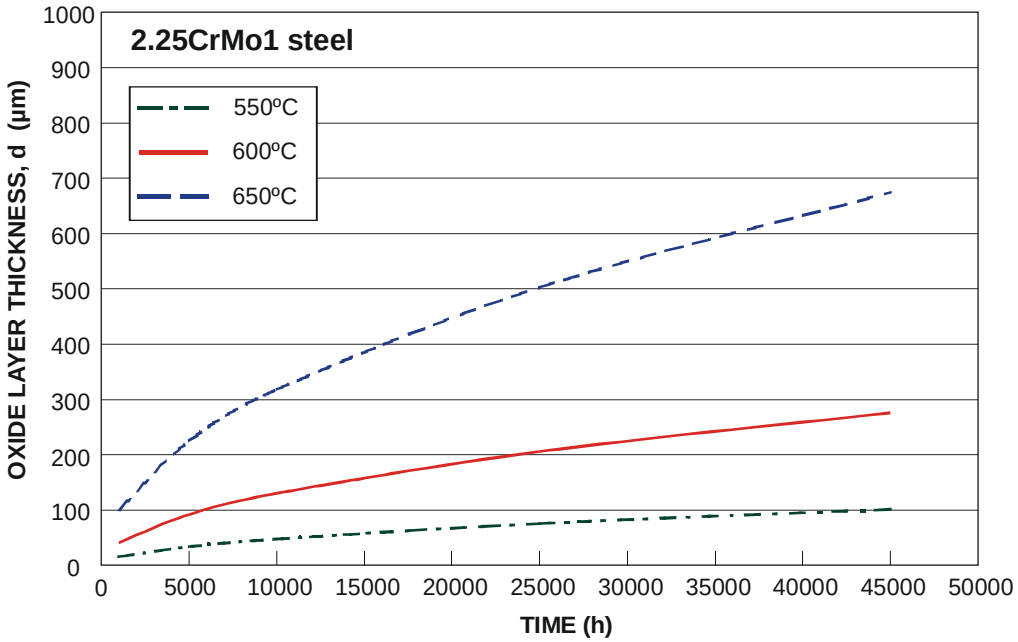

Fig. 4: Oxidation kinetics, oxide layer growth d, of ferritic 2.25 % Cr-steel under steam at 560–700°C using Arrhenius equation type curve fitting and extrapolation to 45,000 h, original data from [30].

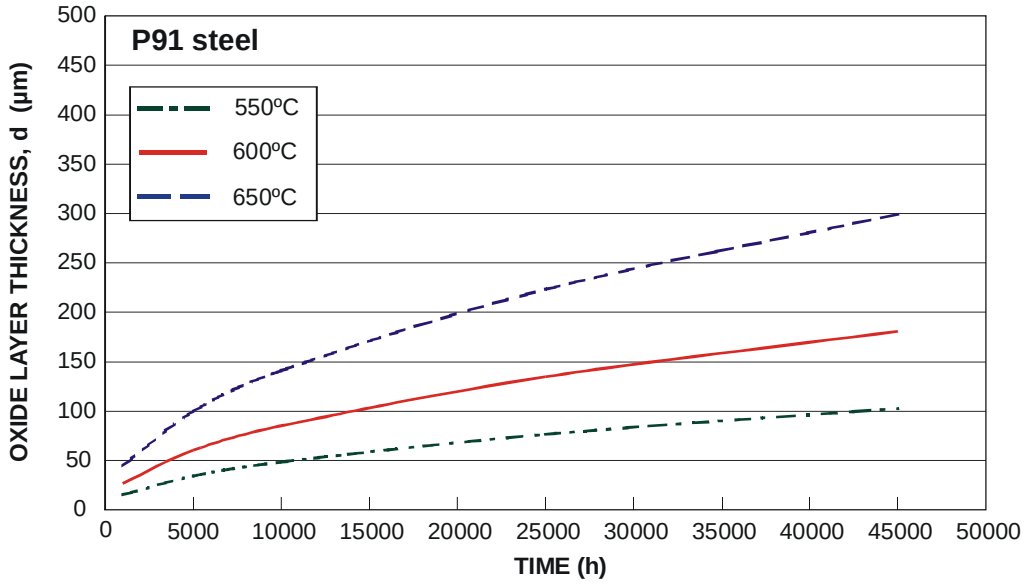

Fig. 5: Oxidation kinetics, oxide layer growth d, of f/m 9 % Cr-steel (P91) under steam at 560–700°C using Arrhenius equation type curve fitting and extrapolation to 45,000 h, original data from [30].

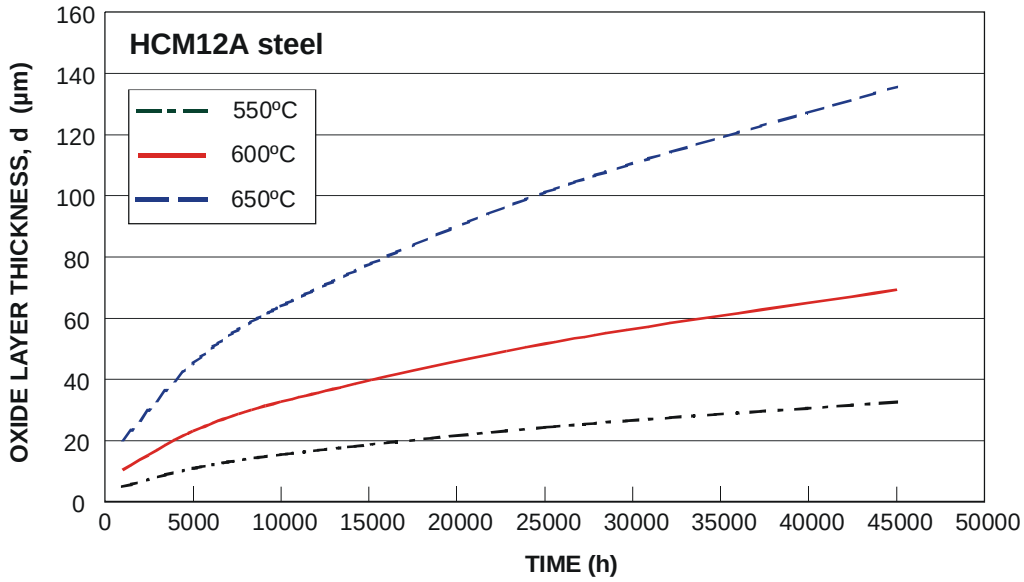

Fig. 6: Oxidation kinetics, oxide layer growth d, of f/m 12 % Cr-steel (HCM12A) under steam at 560–700°C using Arrhenius equation type curve fitting and extrapolation to 45,000 h, original data from [30].

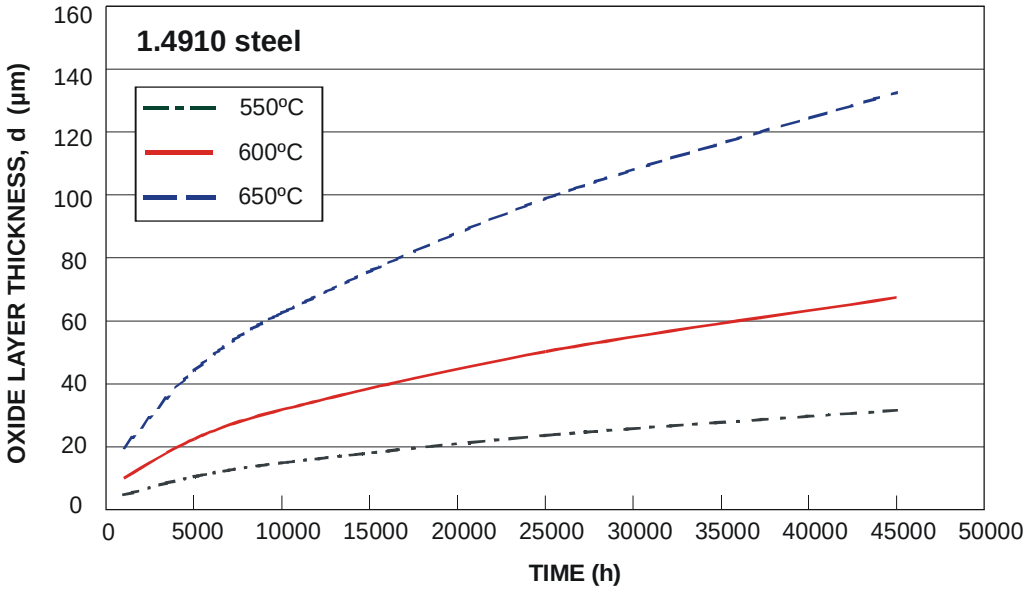

Fig. 7: Oxidation kinetics, oxide layer growth d, of austenitic 18 % Cr steel (1.4910) under steam at 560–700°C using Arrhenius equation type curve fitting and extrapolation to 45,000 h, original data from [30].

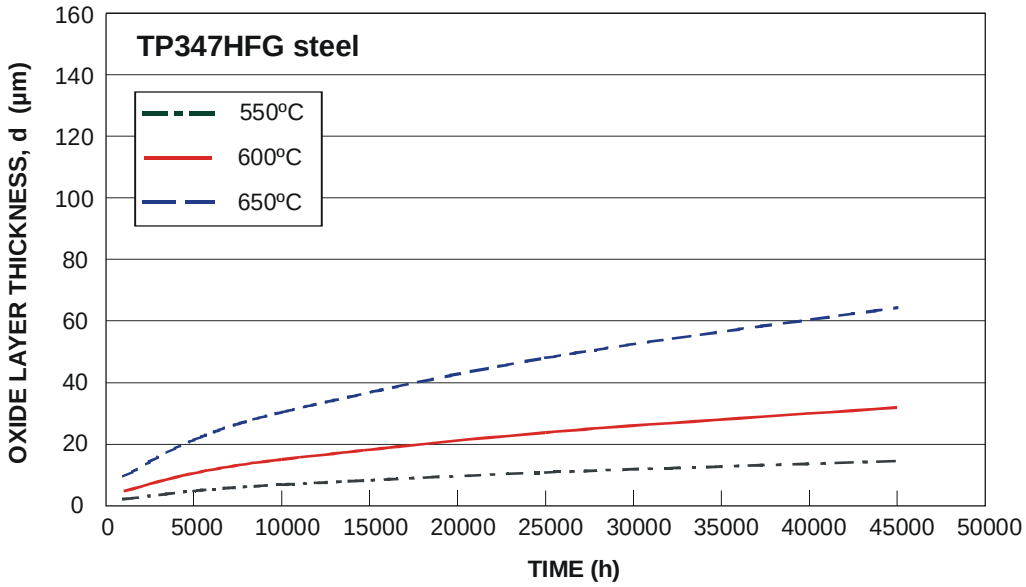

Fig. 8: Oxidation kinetics, oxide layer growth d, of austenitic 18 % C, 10% Ni and 1 % Nb steel (TP347 HFG) under steam at 560–700°C using Arrhenius eq. type curve fitting and extrapolation to 45,000 h, original data from [30].

3.3.2 Oxidation of Ni-based alloy Inconel 625

The oxidation rate of the Ni-alloy Inconel 625 was found to be negligible [34]. For 45,000 h at 621°C, the metal loss of Inconel 625 is less than 15 µm, extrapolated from Fig. 9.

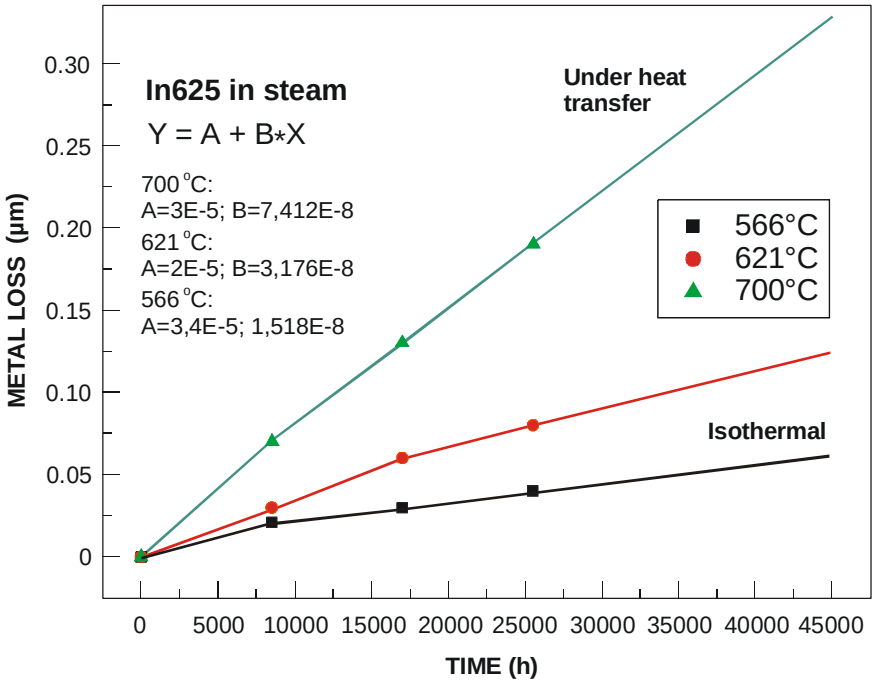

Fig. 9: Oxidation kinetics of Inconel 625 in steam under heat-transfer (700°C) and isothermal conditions (621–700°C). Extrapolation from 3,600 h (heat-transfer) and 10,000 h isothermal exposures with Origin 6.0, from [34].

3.4 Comparison of general corrosion in water and steam

The knowledge of the oxide layer thickness on structural components like fuel pins is essential for the calculation of the mechanical integrity (e.g. cladding thickness) under the burnup conditions of the fuel. For a correct design of HPLWR components, data regarding the oxidation behavior of materials in supercritical water should be used. As mentioned above, such data are very rare for HPLWR-relevant materials and operational conditions in the literature. Boyd et al. published a comprehensive overview on the corrosion behavior of ferritic and austenitic steels and some nickel-based alloys in degassed water at 345 bar and 427, 538 and 732°C over up to 3,500 h of testing [24]. They evaluated a linear time law for the corrosion kinetics (see Eq. 2), which indicates that no protecting layers were formed during the exposure in pure water, with activation energies of about 132.5 for TP347 HFG and 59.1 kJ/mol for SS410. These data were gained in the late 1950s and hence their experimental accuracy and relevance to today's applications like HPLWR is rather difficult to estimate.

Therefore, data from steam oxidation are typically used for the selection of appropriate materials in the power generating business (LWR and non-nuclear systems) as shown in Figs. 4-8 and expressed by Eq. 3 and 4. For a 12 % Cr-steel (HCM12A) at temperatures ranging between 550 and 650°C, oxide layer thickness of about 35 to 135 µm can be determined from Fig. 6, whereas for a 18-10 CrNi steel (TP347 HFG) ca. 15 to 65 µm (Fig. 8) can be calculated for an end-of-life period of 45,000 h. The corresponding activation energies are 90.1 for HCM12A and 94 kJ/mol for TP347 HFG.

An extrapolation of the oxide layer thickness on HCM12A and SS 347 to longer times (e.g. up to 45,000 h), evaluated from "water" data [24] and a comparison with "steam data" [30] for equal temperatures is rather difficult, because of the uncertainty of the short-term water experiments of Boyd et al. (only ca. 3,500 h). Furthermore, due to the different activation energies and the fact, that different time laws (linear for water and parabolic for steam) are valid, a comparison of both sets of data did not lead to a convincing conclusion. Future corrosion experiments in supercritical water have to provide a more reliable database.

3.5 Stress corrosion cracking (SCC)

A review of the SCC behavior of the above-mentioned material groups has to take into account that two different cracking phenomena exist:

- the intergranular and
- the transgranular crack formation

They are caused by electrochemical corrosion mechanisms of detrimental interaction between material, medium and stress. Parameter of influence on both kinds of cracking are mainly the composition and metallurgical condition of the material of interest, the medium in respect to its composition and physical state and the mechanical load, i.e. the applied stress level defined by percentages of Rp_{O2}, during material application. All these conditions are simulated as closely as possible by the chosen testing methods.

The test results are frequently difficult to interpret when main parameters are overdone to accelerate the corrosion process. That brings us away from reality in engineering.

Analyzing the behavior of the main HPLWR material groups, major SCC differences have to be taken into account. They are caused mainly by the very different nickel contents of the alloys under consideration. While the common austenitic CrNi-steels fail transgranular in chloride containing aqueous media, high-nickel steels are sensitive to intergranular stress corrosion, even under stress in pure water.

The broad minimum band of “passivity” or “immunity to both kinds of failure modes” in the diagram of J. Blanchet and H. Coriou [37] (Fig. 10) goes from about 20 to 60% nickel content of the high temperature alloys. It reveals the above mentioned difference of corrosion danger for low and high nickel containing alloys, but also shows the potential resistivity against SCC within the given limits, e.g. for Incoloy 800 (32% Ni) and Inconel 690 (58% Ni). These alloys are applied with success in PWR’s or other reactor systems as main representative materials for steam generation [38].
Figure 11 shows the dependence of stress corrosion cracking in SS 304 as a function of oxygen and chloride content in water with metallurgical condition, varied by different heat treatments, as parameter. Higher sensitivity goes along with the formation of chromium-rich precipitates at grain boundaries and leads to intergranular stress corrosion cracking (IGSCC), also in common austenitic stainless steels. In BWR’s, both in pipings as well as in structural core components IGSCC has been detected in several austenitic stainless steels. There exist two possibilities to decrease sensitization, either to use low carbon variants or to apply so-called stabilized alloys, in which the carbon content is bound by the formation of intragranular MC-precipitates. This has an additional positive effect on the strength of alloys. The experience with niobium- and titanium stabilized alloys like 1.4541 (AISI 321) and 1.4550 (AISI 347) in LWR’s is generally very good and occasionally found defects in the weldments and heat affected zones (HAZ) of pipings and core containments in BWR’s were due to incorrect heat treatment [39-40]. These findings let us assume that by an appropriate choice of alloy composition and heat treatments, besides the use of low O_2/Cl^- media, the range of insensitivity to SCC can be expanded to conventional austenitic stainless steels with lower nickel content for use in HPLWR. The specific interest in low Ni-containing austenitic stainless steels is based on the high neutron absorption of nickel, which needs higher enrichments of fuels.

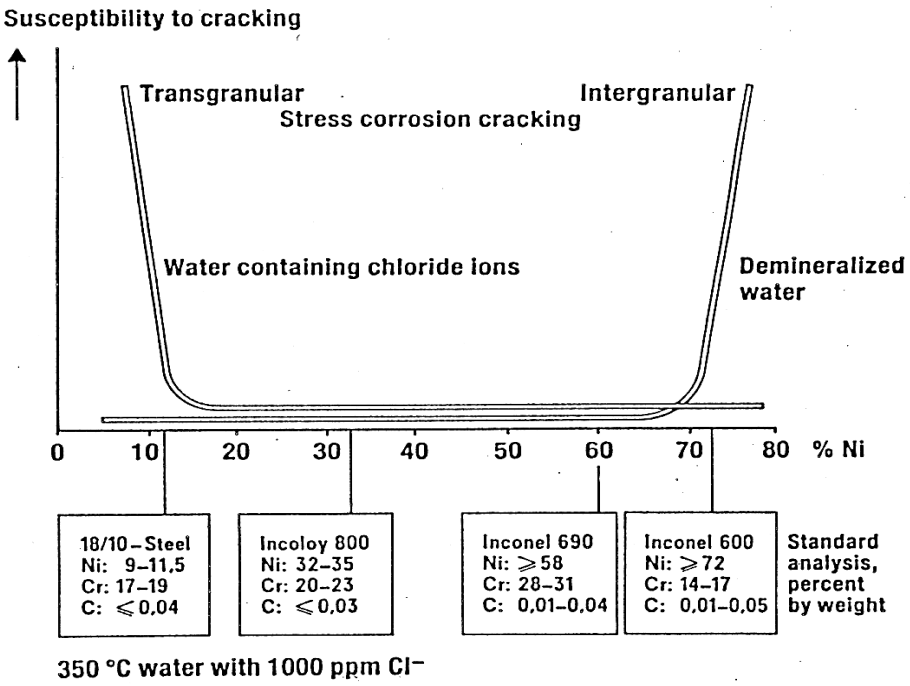

Fig. 10: The sensitivity of steels and Ni-alloys to SCC in dependence of nickel concentration [37]

For future HPLWR reactors, materials are of interest, which are resistant against SCC in the temperature range between 300 and 650°C. Unfortunately, results on SCC in supercritical water (SCW) are very scarce. Nevertheless, some interesting data are available in the literature although they don't correspond exactly to the HPLWR's case.

Boyd et al. [24] have presented two SCC tests at constant stress in a static autoclave filled with degassed deionized supercritical water at 732°C. Two materials have been tested: 316 (at 103 MPa) and 347 (at 82 MPa) stainless steels. There was no rupture after 1 month for 347 and rupture after one week for 316. Transgranular cracks associated with corrosion pits were found. This finding confirms the above statement that stabilized stainless steels are promising materials.

In his thesis, Fournier [41] has studied the SCC of Alloy 690 and Alloy 718. Slow Strain Rate Tests (SSRT) were used to evaluate SCC susceptibility. A strain rate of 10^{-6} s^{-1} was used. The tests were carried out in deionized water (18 MΩcm) at 400°C and 250 bars. In addition, tests were achieved in air in order to prove that eventual rupture in water is due to SCC and not to pure mechanical effects. Fig. 12 shows the deformation/stress diagram for Alloy 718 in supercritical water and air. One can observe that elongation at failure is much lower in water than in air. The investigations by Scanning Electronic Microscopy (SEM) reveals intergranular zones on the fracture surface. It was concluded that Alloy 718 is sensitive to SCC at 400°C in pure water. Same tests have been carried out with Alloy 690. The results are different. It can be seen in Fig. 13 that deformation/stress diagram in supercritical water and air are rather similar. It should be noticed that the strain rate (10^{-6} s^{-1}) is perhaps a little bit too high to prove the non-sensitivity of Alloy 690. Nevertheless some nickel-based alloys also seem to be promising materials.

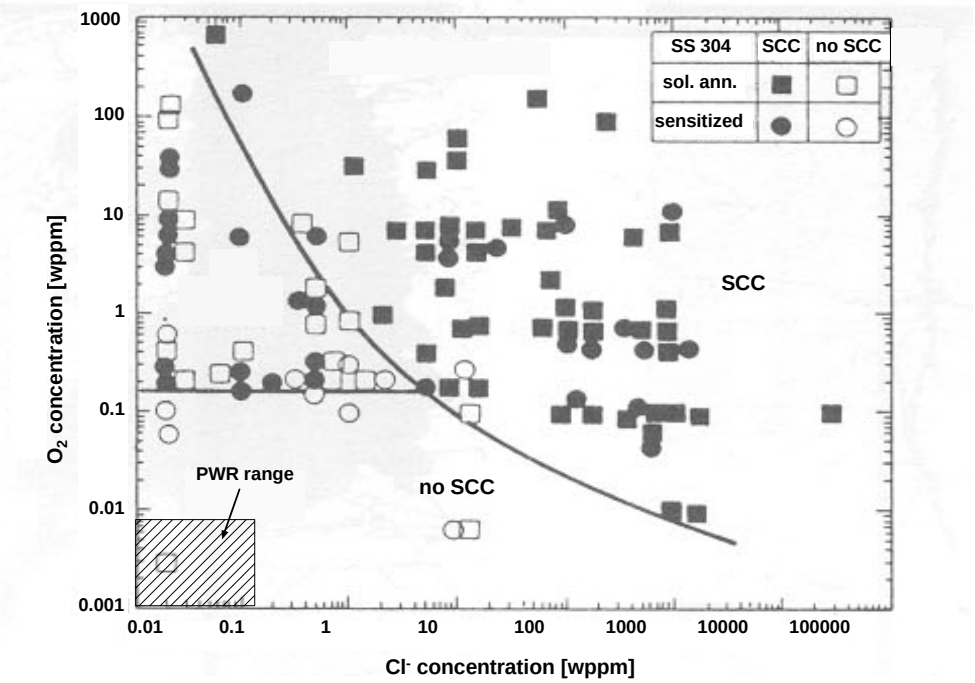

Fig. 11: The effect of O_2 and Cl-content on the stress corrosion cracking of SS304 in subcritical water [Sedriks-Wiley Interscience 1979 and B.M. Gordon 1980]

Many parameters may modify SCC in supercritical water: H_2/O_2 content, Cl^- content, residual compressive stress due to grinding, microstructure (inclusion, grain size) or chemical composition. It needs of course several experiments to evaluate the effect of such parameters. For example, screening tests in an autoclave with C-ring, U-bend, etc. at constant deformation is an inexpensive way to test several samples at the same time. With such kind of tests, one can study:

- ♦ Different materials: stainless steels (stabilized or not), nickel base alloys, 9-12% Cr ferritic-martensitic steels
- ♦ The effect of dissolved hydrogen
- ♦ Compressive surface residual stresses obtained by grinding
- ♦ The effect of microstructure

It was also confirmed, that the 9-12 % Cr ferritic/martensitic steels are more resistant to SCC and IASCC than austenitic stainless steels in both, unirradiated and irradiated conditions [42].

In summarizing, it seems that regarding the SCC phenomena, the group of 9-12 %Cr steels, conventional stabilized austenitic steels and higher chromium and nickel variants like Incoloy 800, as well as specific Ni alloys like Inconel 690 promise the best behavior.

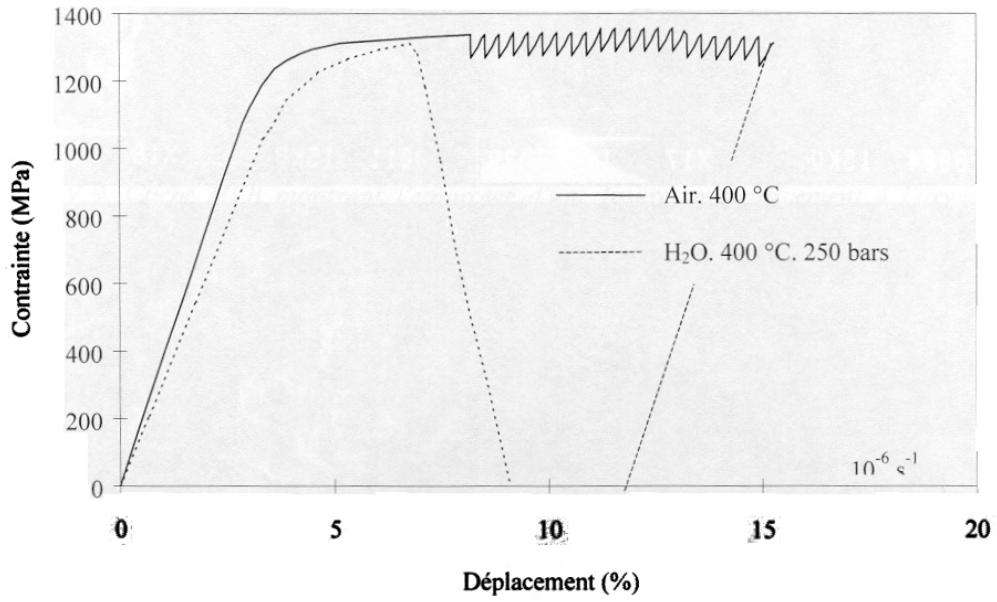

Fig. 12: Slow Strain Rate Test on Alloy 718 - Stress (MPa) versus displacement (%) after [41]

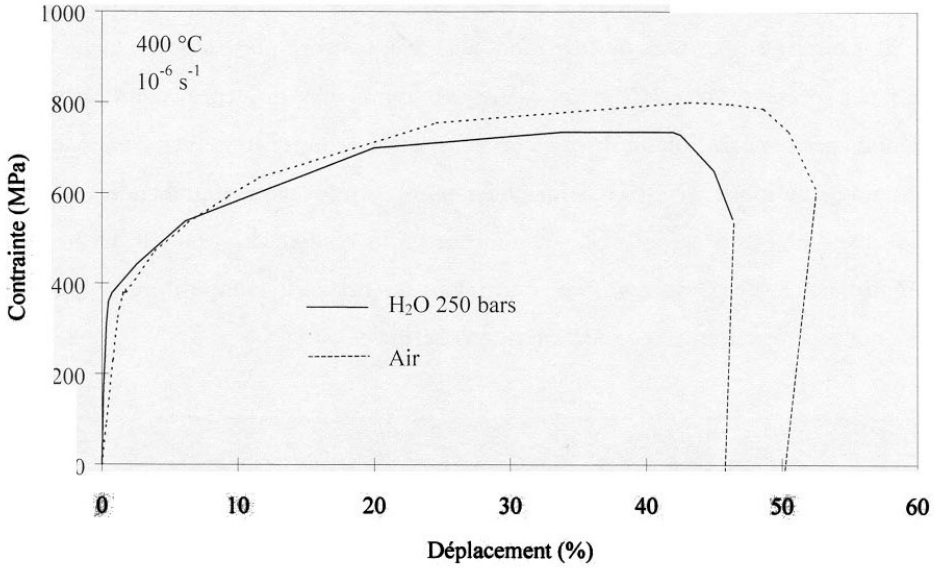

Fig. 13: Slow Strain Rate Test on Alloy 690 - Stress (MPa) versus displacement (%) after [41]

4. Investigations on In-vessel materials

4.1 Selection of appropriate material groups

The selection of in-vessel materials is based on conventional properties, on their technical availability and ripeness and on existing experience in nuclear environment. Table 9 gives a survey on three major groups of materials, which in principle have the potential for application in an HPLWR under supercritical water conditions. Classical Zr-based alloys are not included, because their creep-rupture behavior does not allow to go far beyond the temperature ranges used in conventional LWR's.

The first group of materials belongs to the **9-12% CrMoVNb ferritic/martensitic (f/m)** steels, which are extensively used in modern steam power plants as pipings and in turbines as rotor and blade materials for temperatures up to 580°C [15]. From a metallurgical point of view these materials are used in a tempered martensite condition, which provides high creep strength and sufficient fracture toughness properties in the envisaged temperature window. The alloy P 91 is the modern variant of a piping material in conventional power plants. This material group also has been used as wrapper material in fuel elements of Fast Breeder Reactors (FBR's). Alloys of types 1.4914, EM 10 and FV448 have shown an excellent irradiation behavior in the temperature range of 400 to 550-600°C. They were not sensitive to swelling and helium embrittlement up to a neutron exposure of more than 100 dpa [42-43]. MANET II is the optimized version of these Nb-stabilized 9-12% Cr steels tested in nuclear environment. A still open point for this material group is a possible irradiation-induced embrittlement, which eventually causes a shift of the ductile-to-brittle transition temperature (DBTT) into the temperature range of 250-300°C.

At present, in the frame of the material development for fusion technology, alloys of type **8-10%CrWVTa** are under investigation, which promise improved fracture toughness over the whole temperature range of interest and especially a lower ductile-to- brittle transition temperature. A very attractive feature of these alloys is a reduced long-term radioactivity and nuclear afterheat, which has been achieved by a tailored chemical composition [44]. EUROFER 97 is the European reference material for the Fusion Reactor Project. The tensile and creep-rupture properties are comparable with those of the conventional alloys P91 and MANET II so that their present temperature window for application is restricted to about 580°C. On a long term there exists a possibility to improve the creep-rupture properties of EUROFER further by strengthening it with Y_2O_3- dispersoids (EUROFER-ODS) [45].

Table 9: Typical chemical composition in wt.-% for candidate in-core HPLWR materials (balance: Fe or Ni)

	MANET-II a	P91 b	1.4970 c	1.4909 d	Incoloy 800 e	PE16 f	Inconel 625 g	Inconel 718 h
C	0,10-0,12	0,06-0,15	0,08-0,12	0,015-0,030	0,05-0,10	max. 0,1	max. 0,10	max. 0,08
Si	0,10-0,30	0,18-0,56	0,3-0,55	≤ 0,5	≤ 1,00	max. 0,3	max. 0,50	max. 0,35
Mn	1,0-1,15	0,25-0,66	≤ 2,0	1,6-2,0	≤ 1,50	max. 0,2	max. 0,50	max. 0,35
P	<0,005	≤ 0,025	≤ 0,015	≤ 0,025	≤ 0,030		max. 0,015	max. 0,015
S	<0,005	≤ 0,012	≤ 0,015	≤ 0,015	≤ 0,015		max. 0,015	max. 0,015
Cr	10,0-10,8	7,90-9,60	14,5-15,5	17-18	19-23	15-18	20-23	17-21
Ni	0,50-0,70	≤ 0,43	14,5-15,5	12-12,5	30-35	42-45	Bal.	Bal.
Mo	0,50-0,65	0,80-1,10	1,0-1,40	2,3-2,7	0,031	2,5-4,0	8-10	2,80-3,30
V	0,15-0,25	0,16-0,27	0,05					
Nb	0,10-0,20	0,05-0,11	≤ 0,02				3,15-4,15	4,75-5,50
B	0,007-0,009		0,003-0,008	≤ 0,020		max. 0,005		max. 0,006
N	0,03-0,04	0,025-0,080	≤ 0,015	0,06-0,08	0,018			
Al	<0,02	≤ 0,05			0,15-0,60	0,9-1,5	max. 0,40	0,40-0,80
Zr	0,015-0,035							
Ti			0,3-0,55		0,15-60	0,9-1,5	max. 0,40	0,65-1,15
Co			≤ 0,03	≤ 0,25		max. 2,0	max. 1,0	max. 1,0
Cu			≤ 0,05	≤ 0,3	≤ 0,75		Fe max. 5,0	Fe 16-18

The second group of materials comprises high-temperature strength **austenitic stainless steels** of Fe-(15-25%)Cr-(10-35)NiMoTi/Nb steels. Alloys such as 1.4970,

also known as 15Cr15NiTi, 1.4909 or 316 LN, and Incoloy 800 belong to this category.

Alloy 1.4970 is a Ti-stabilized material with excellent creep strength, which has been tested in several chemical modifications as cladding material in European FBR's with good success up to 150 dpa [43, 46]. Alloy 316 LN has been used in a nuclear grade version as reactor vessel steel in FBR's in lower neutron fluence regions and is also foreseen as structural material for the International Thermonuclear Experimental Reactor (ITER). This alloy, in the solution-annealed condition, might be limited to moderate fluence levels in the range of 30 dpa. Alloy 800 is a high chromium and nickel containing, Ti-stabilized austenitic steel with excellent corrosion behavior and is used very successfully in nuclear steam generators [47]. For Alloy 800 the experience under neutron irradiation is less extensive. Unlike for the f/m steels the possibility to develop **low or reduced activation variants** is limited for the austenitic stainless steels.

The third group of materials selected in Tab. 9 are **Ni-based alloys**. PE 16 is a-γ-prime precipitation-hardened alloy with a high creep strength. It has extensively been tested with success as cladding material in the European Fast Breeder Reactor project [43]. However, there exist no reliable data on corrosion resistance in water for this material. Inconel 625 and Inconel 718 have typical nickel–based compositions, are also γ-prime hardener and are used as structural parts in LWR's and as cladding and structural components for in-core materials in FBR's. These alloys show a high creep strength and low corrosion rates in steam environment. However, dependent on the detailed chemical composition they can be very sensitive to stress corrosion. Irradiation effects like swelling and irradiation-creep are generally low in the temperature range of 400 to 650°C up to fluence levels of about 150 dpa. Due to high helium production via a Ni-double transmutation reaction and an inherently high matrix strength, the alloys are generally prone to high temperature helium embrittlement, which is manifested by a strong tendency for intergranular fracture along grain boundaries. In a thermal neutron spectrum this sensitivity to helium embrittlement should further increase. Since nearly all alloying elements have absorption cross-sections for thermal neutrons much larger than 1 barn, their extensive use in a thermal nuclear core would need a larger enrichment of the uranium fuel to balance the neutron economy. Also the high content of Nb, Mo, Ta and W in these alloys leads to a high neutron-induced long-term activation. Therefore, a development of low-activation Ni-alloys is not possible.

4.2 Material properties

Unirradiated mechanical properties

For the design of fuel elements and other in-core components tensile and creep-rupture properties are of utmost importance. Therefore, the data of some alloys selected from those listed in Table 9 are compiled. Figs. 14 and 15 show the yield strength ($R_{P0.2\%}$) and ultimate tensile strength R_m of four alloys in different thermo mechanical treatments. The f/m steel MANET II is in a normalized and tempered condition, 1.4970 is solution annealed and 20% cold-worked, PE 16 is solution-annealed and aged and the data of Inconel 625 refer to the solution-annealed state. Figs. 16 and 17 give the so-called 1%-creep yield strength limit ($R_{P1\%/45\ 000h}$) and the

creep-rupture strength $R_{m/45\ 000h}$) after 45,000 h in comparison. The creep-rupture data of Incoloy 800 refer to a solution-annealed state, whereas those of Inconel 718 belong to a solution-annealed and aged pretreatment. The thermo mechanical treatments of MANET II and 1.4970 are the same as for the tensile properties. In Fig. 18 the creep-rupture strength of the ODS-strengthened alloy EUROFER (normalized and tempered) is compared with that of the f/m steel EUROFER. The comparison indicates that with this material the maximum temperature can be increased by about 100°C.

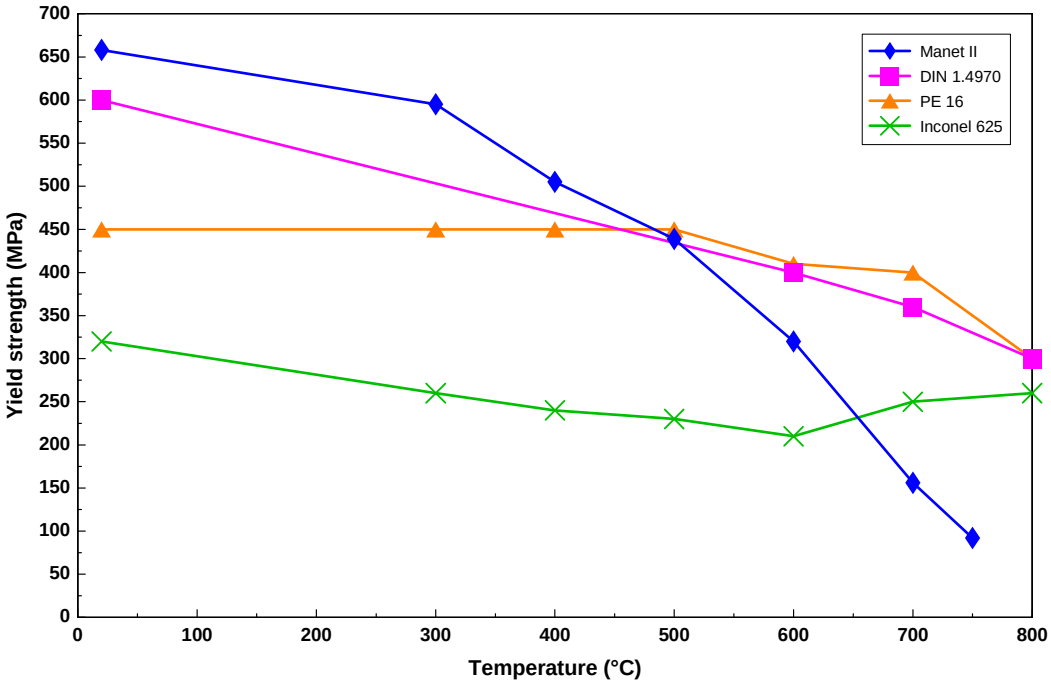

Fig. 14: Yield strength $R_{P0.2\%}$ for selected alloys as a function of temperature

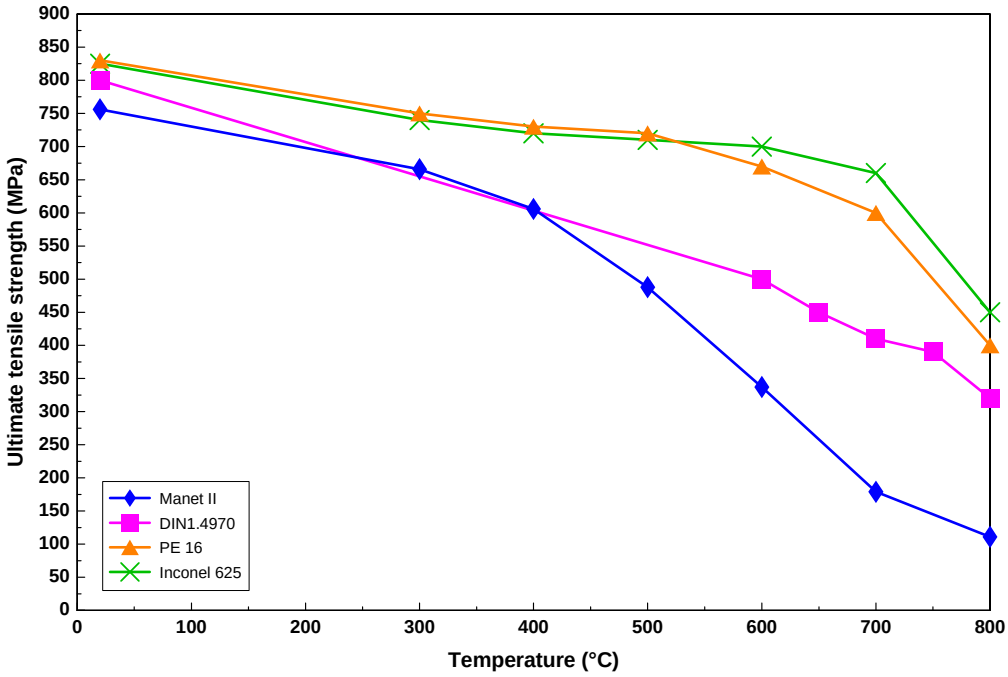

Fig. 15: Ultimate tensile strength R_M for selected alloys as a function of temperature

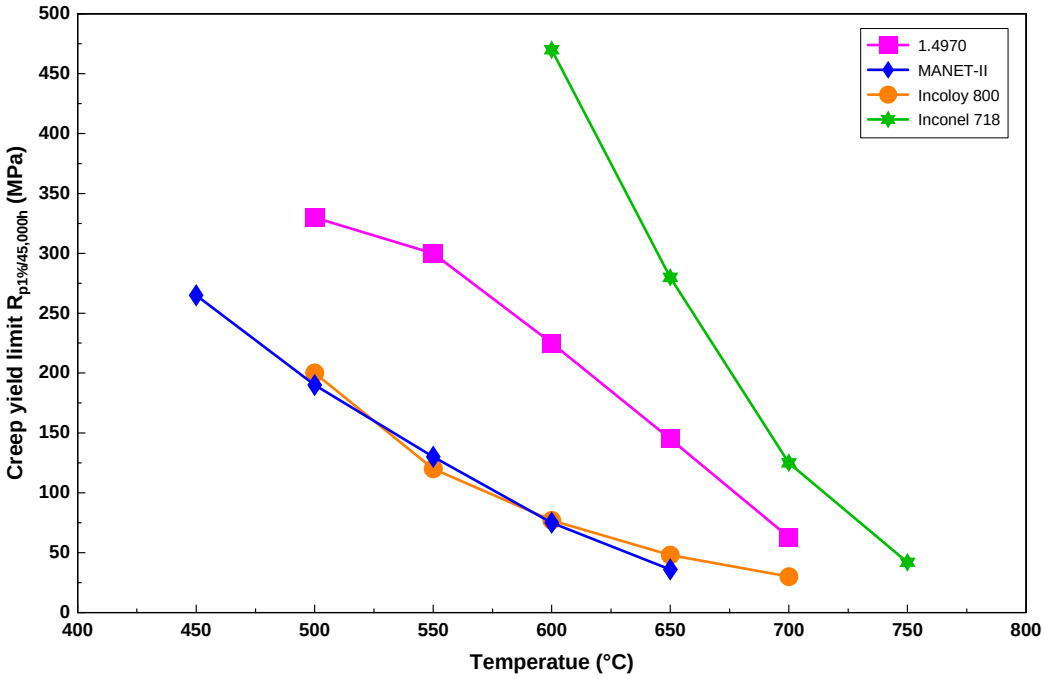

Fig. 16: 1% Creep yield limit $R_{P1\%/45,000h}$ for selected alloys

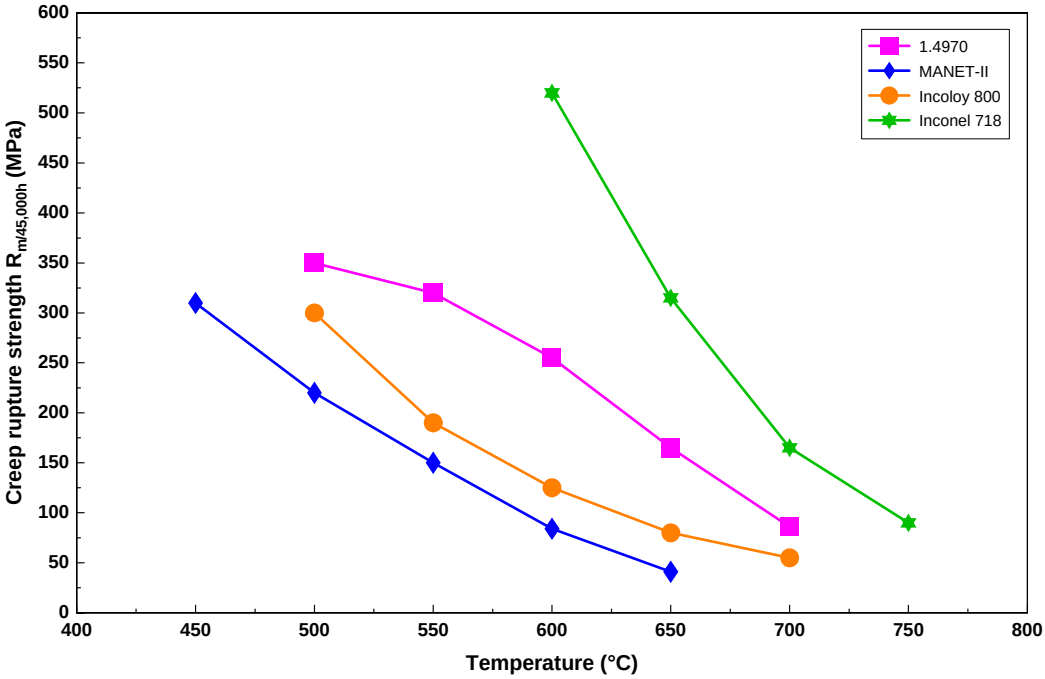

Fig. 17: Creep-rupture strength $R_{M/45,000h}$ for selected alloys

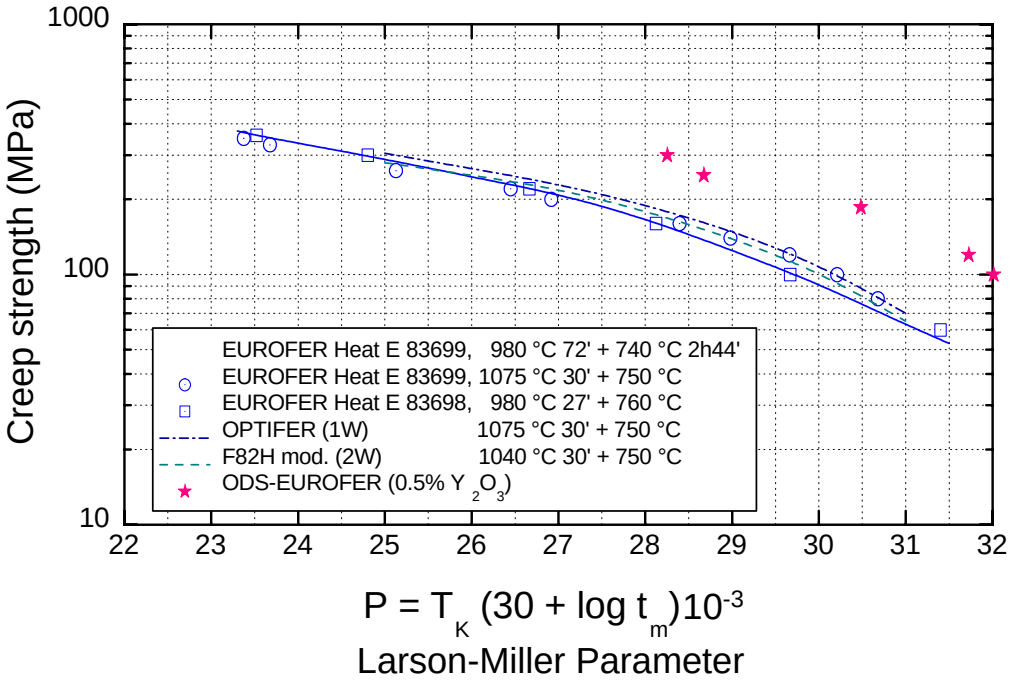

Fig. 18: Comparison of creep-rupture strength R_M for EUROFER and EUROFER/ODS in Larson – Miller diagram

Mechanical properties after irradiation

It is generally observed that the yield strength of steels and Ni-alloys increases if irradiated below a certain temperature and comes to saturation at intermediate neutron fluence levels (5-20 dpa). Fig. 19 shows this behavior for a series of different austenitic steels [48]. For these alloys irradiation hardening is observed if neutron exposure takes place at or below about 550°C. By this low temperature strengthening the capability for work hardening is generally reduced so that the rupture elongation is limited in this temperature range to few percent. For f/m steels irradiation hardening is observed below about 400-450°C, whereas Ni-alloys behave very similar to the austenitic steels. For f/m steels irradiation hardening leads also to a partially strong increase of the ductile to brittle transition temperature (DBTT) up to a temperature range of 250-300°C, dependent on the material composition. Below DBTT the fracture toughness is low, so that these alloys are not applicable below this temperature.

As a consequence for the design, the unirradiated strength data are conservative, but a limit for plastic deformation (usually 0,5%) has to be set for the irradiated materials in this temperature range.

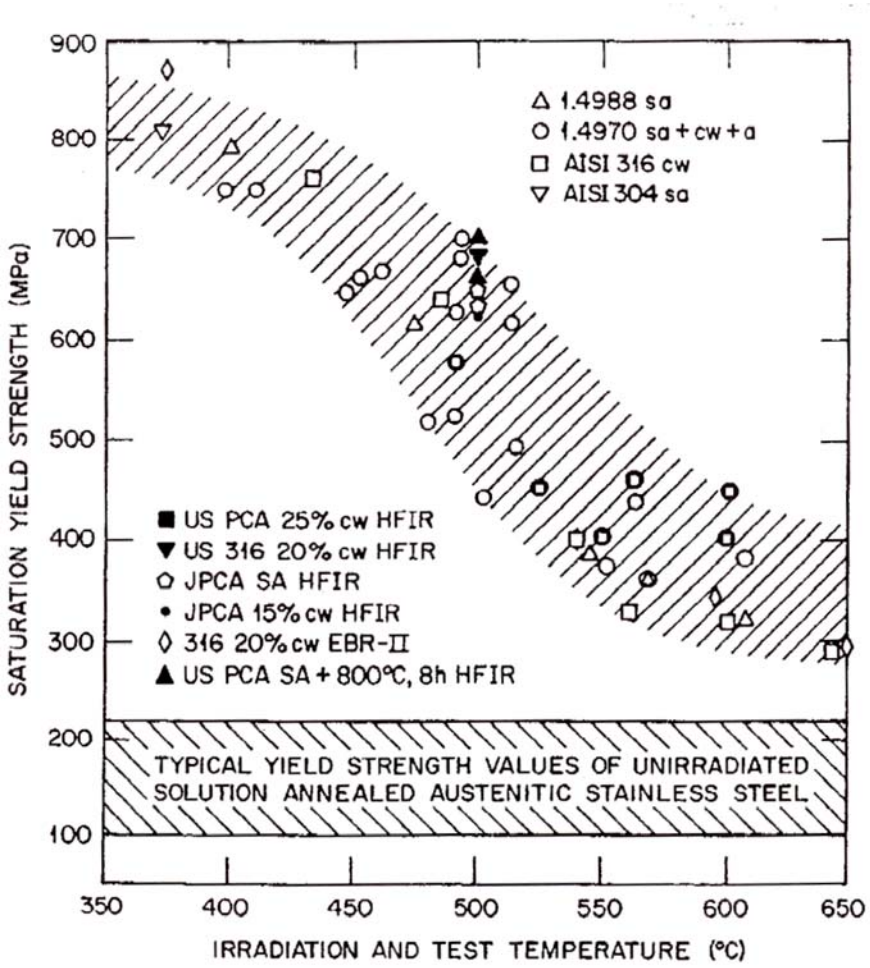

Fig. 19: Saturation yield strength as a function of temperature for austenitic alloys irradiated in different reactors [48]

At higher temperature (above about 0.45 of the melting temperature), which corresponds to about 550°C for steels and Ni-alloys, a different type of embrittlement, which is not connected with an increased strength, can often be observed especially in austenitic steels and Ni-alloys. It is caused by the formation and unstable growth of helium bubbles at grain boundaries, which leads in many cases to a reduction of the rupture time in post-irradiation creep-rupture tests. This reduction is strongly dependent on material, material pretreatment and stress level or deformation rate. For the alloy 1.4970 it is on the order of 20-30 % when compared with the unirradiated material. Therefore, it is generally recommended to increase the safety factor or to limit the creep ductility – e.g. to a value around 1% - which corresponds to the 1% creep yield limit in Fig. 16. In-reactor creep-rupture tests are very scarce and differ strongly in their results. Dependent on material similar or even stronger reductions of lifetime are reported in the open literature. Also, there exist different views about the dominant creep mechanism above about 550-600°C during irradiation.

Swelling and irradiation creep

Swelling and irradiation creep are typical phenomena observed under irradiation. Both are induced by a separation of irradiation–induced vacancies and interstitials into voids and planar loops. Dependent on temperature, flux and fluence level they

can lead to dimensional changes and bowing of core structures. Whereas the swelling is very sensitive to the specific chemical composition and thermo mechanical pretreatment of a material, irradiation creep shows less variability.

The swelling starts for the materials MANET II, 1.4970 and PE 16 in the treatments and compositions mentioned before, after a neutron fluence nearby the maximum 60 dpa level to be expected in the HPLWR [43, 49]. Up to 1.5 % volume swelling can be expected, which corresponds to a linear swelling of 0.5 %.

There is clear evidence in the literature that this value can be further increased, if stress is applied to the material. Assuming the following formula,

$$\Delta V / V_o(\phi t, \sigma) = \Delta V / V_o(\phi t, \sigma = 0) \cdot (1 + A\sigma_{Hyd}) \tag{5}$$

the additional contribution to swelling by stress can be estimated by the term $A\sigma_{Hyd}$. The constant "A" determined from many experiments is in the range of $1\text{-}3 \cdot 10^{-3}$ [MPa^{-1}], so that with a hydrostatic stress component of 100 MPa the stress free swelling has to be increased by 10–30 %. Even, if over the whole length of fuel pins the maximum neutron dose of 60 dpa would be achieved the general limit of 1% linear swelling would not be exceeded. Some uncertainty lies, however, for this estimation in the fact that the helium generated per dpa is higher for the HPLWR neutron spectrum when compared with a typical FBR spectrum, from which all swelling data are received.

Irradiation creep is a novel process of deformation, which has been observed in practically all materials under irradiation. It is characterized in contrast to thermal creep by a nearly linear stress dependence and only a very small temperature dependence. It appears generally below about 0.55 $T_{Melting}$ for neutron flux levels typical for LWR´s and FBR´s. In absence of swelling the stress-normalized irradiation creep rate per dpa can be described by:

$$\varepsilon / \sigma = \text{SIPA} \cdot \text{dpa} \tag{6}$$

The SIPA coefficients [MPa^{-1},dpa^{-1}] for the alloys 1.4914 (f/m steel), 1.4970 (austenitic stainless steel) and PE 16 lie in the range of $1 \cdot 10^{-6}$ (1.4914 and PE 16) to $2.5 \cdot 10^{-6}$ (1.4970). An additional contribution to irradiation creep by swelling – the so-called I-creep - as has been observed for high dpa levels can be neglected for the case of HPLWR. From principle reasons it is assumed that a deformation caused by SIPA- and I-creep does not lead to fracture-except that the deformation allowed by irradiation creep is limited from geometrical reasons.

A critical question is, at which stress level and temperature range SIPA-irradiation creep is substituted by thermal creep, which has a much higher stress exponent and a strongly accelerated creep rate. This range has not been fully investigated by experiments. For instance in material 1.4970 at 420 and 500°C SIPA creep was experimentally confirmed for stress levels of 60 and 120 MPa, whereas at 600°C only for 60 MPa the same deformation mechanism was observed, whereas at 120 MPa a strongly increased creep appeared, which was neither linear in stress nor in dose (dpa) and led to a rupture of pressurized tubes above 60 dpa. It is assumed that the upper stress/temperature range for irradiation creep increases with the thermal creep-rupture strength of a material, so that for a given stress level the temperature,

at which a transition from irradiation creep to radiation enhanced thermal creep occurs, increases from f/m steels to austenitic stainless steels and Ni alloys. For a system like in HPLWR very high operational stresses in the cladding material should be avoided by adopting a larger cladding thickness.

Compatibility of fuel pin claddings with uranium dioxide

A possible incompatibility with UO_2 is another limiting factor in designing claddings for fuel pins. The investigations of fuel elements used in Material Test Reactors and FBR´s cover a broad range of burnups (max. 20 at.-%), neutron spectra (thermal, epithermal, mixed thermal/fast and fast) and rod power (200-800 W/cm) [46]. From thermodynamic reasons, only chromium which-besides iron and nickel-is a major alloying element for all cladding materials compiled in Table 9 can be oxidized by UO_2. Up to a cladding temperature of 700°C these alloys form a very small and stable oxide film, if in contact with virgin fuel. With increasing burnup the presence of fission products like Cs and Te changes this behavior and irradiated fuel can attack the material above about 550°C cladding temperature. The observation of clad attacks by inner corrosion shows, however, a widespread picture and corrosion attacks from few μm up to 230 μm are reported in the literature. The majority of observations lies in the range of 50-100 μm. Unfortunately there are only few parameters from which one can definitely say that they promote the clad attack: these are a low fuel density (85-90 %TD) and a high rod power, hinting at a quick release of Cs and Te to the cladding inner surface. The systematic investigation of materials from austenitic stainless steels via higher alloyed steels like Incoloy 800 and the Ni alloy Inconel 625 did not show a strong variation of inner corrosion with composition. The only exceptions were claddings made of austenitic stainless steels with a very low Cr- concentration on the order of 9-10 %. This can be understood from the general experience that in ferritic and austenitic stainless steels about 12% Cr is necessary for the formation of a protective Cr_2O_3 layer.

In order to estimate for the fuel clad design the effect of inner corrosion on the diminution of the cladding thickness, in the following Chapter 5 it is tentatively proposed to investigate the following kinetic equations, whereby it is assumed that at a burnup of 70 GWd/t_U, which corresponds to about 7 at-%, a maximum corrosion attack of 70 μm will be achieved:

$$\Delta d[\mu m] = 1.5E-3 \cdot t[h] \quad (7)$$

$$\Delta d[\mu m] = 0.3299 \cdot \sqrt{t} \quad (8)$$

These equations reflect the observation that the experimental results do not always suggest a linear dependence of inner corrosion with burnup or time (Eq. 7), but an early accelerated incompatibility with tendency of later saturation (Eq. 8).

There is a further possibility of damaging the cladding, which is connected with the formation of the halogens J, Cl and F during burnup [50-51]. In corrosion experiments with halogen-containing simulation products at 400 and 500°C it was shown that for unstressed specimen the corrosion attack was small in austenitic stainless steels and Inconel 718, whereas under stress the Ni alloy was cracked and the austenitic steels

remained intact. These results cannot be further quantified at the moment, but show the role of halogen elements for a possible stress corrosion cracking.

In concluding, the major uncertainties in the assessment of in-core materials are, besides the corrosion under supercritical water conditions the mechanisms which lead to deformation under irradiation at high stress levels, and-for the claddings-in addition the role of fission products for their integrity.

5. Estimation of temperature range and cladding dimensions of fuel pins based on creep-rupture, corrosion and compatibility properties

In Table 1 the initial reference design data of Oka [2] and more ambitious operational conditions for the in-core fuel element assemblies [5-6] have been compiled. They include an extension of burnup and lifetime of fuel pins and reasonable assumptions on a technically possible pin pressurization and fission gas release. This allows a more detailed calculation of the stress development in fuel pin claddings.

A first calculation with the Kesselformel (KF) to determine the necessary cladding thickness for a hoop stress of 100 and 200 MPa respectively, for a constant maximum differential pressure of 17 MPa and in dependence of the pin diameter (6-10 mm) was presented in the HPLWR Annual Technical Report [1]. In this estimate the cladding thickness depends linearly upon the differential pressure and the cladding diameter and decreases linearly with the “allowable” hoop stress. The results of this calculation, which are independent of specific material properties, are repeated in Table 10.

Table 10: Variation of clad thickness with pin diameter for 100 and 200 MPa stress level

Diameter ϕ [mm]	**6**	**8**	**10**
Wall thickness for 100 MPa	0.51	0.68	0.86
Wall thickness for 150 MPa	0,34	0,45	0,57
Wall thickness for 200 MPa	0.26	0.34	0.43

In LWR fuel pin designs and also in pipings of conventional power plants the equivalent stress level is in the range of 100 MPa. This is a rather moderate value with the advantage that material behavior under these conditions is well established, but is not necessarily a limiting figure if only stress rupture data are taken into account. However, there exist for thin tubes additional conditions, which have to be fulfilled: These are among others a resistance against elastic tube buckling and plastic deformation. The restrictions of pressure level and hence minimum clad thickness are determined below for the case of tube buckling:

The critical elastic pressure for clad collapse $p_{collapse}$ depends on the radial geometry and the elastic modulus E of the cladding material and can, according to Yamaji et al. [52], be calculated by:

$$p_{collapse} = 0.73 \cdot E \cdot \{d / (\phi - d)\}^3 \quad (9)$$

whereby: E = Elastic Modulus
d = Wall thickness
ϕ = Diameter of the cladding

The extreme case for design is the initial differential pressure (17MPa) and the maximum clad temperature at the hot channel (assumed to be 800°C, [52]). At this temperature the E-modulus has the lowest value and differs only slightly with material. For instance the values for three representative candidates of Table 9 are: $1.39 \cdot 10^5$ MPa for MANET II, $1.34 \cdot 10^5$ for 1.4970 and $1.43 \cdot 10^5$ for PE 16. Taking the lowest value for 1.4970 this gives the minimum clad thickness d_{min} necessary to avoid immediate buckling. The calculated values d_{min} are compiled in Table 11 together with the corresponding maximum stress level σ_{max} which can be accepted under these conditions.

Table 11: Minimum clad thickness to avoid buckling

Diameter Φ [mm]	**6**	**8**	**10**
Wall thickness d_{min} [mm]	0.34	0.45	0.56
Stress level [MPa]	150	150	150

A comparison with Table 10 shows that in order to avoid immediate clad buckling for the given conditions the stress level has to be restricted to a level of 150 MPa with a minimum cladding dimension shown in Table 11. One has, however, to mention that a high safety margin of 1/3 is included in the above formula. If no such margin is considered, stress levels of up to 215 bar would be allowed, with the consequence that the d_{min} values could accordingly be diminished.

Therefore, there is still a certain flexibility to vary the equivalent stress level by changing the dimensions of the cladding, which of course has an influence on the maximum achievable operational temperature. This is illustrated in Table 12, where for different candidate materials the maximum temperatures based on their creep-rupture properties for a lifetime of 45,000 hours (Fig. 17) were determined. They show the possible variation with the selected cladding material. As an example, for a 100 MPa hoop stress the following trends can be seen: With the class of ferritic/martensitic 9-12% Cr steels a temperature range of 550–590°C can be achieved. This temperature range would fit well into the presently used circuit parameters of conventional power plants with supercritical steam conditions, where ferritic/martensitic alloys like P91 and 1.4922 are used. However, in the nuclear core higher maximum cladding temperatures are necessary to generate the envisaged coolant outlet temperature.

As expected and confirmed in Table 12 the estimated maximum temperature is higher for the group of investigated austenitic alloys. It varies between 625 and 690°C and is very dependent on the chemical composition of the individual material.

The two nickel-alloys extend this temperature range by further 20-30°C up to 720°C.

If a higher hoop stress level is used (e.g. 200 MPa), the maximum temperatures are reduced by 50°C and more, dependent on the individual creep-rupture data shown in Fig. 17.

In the KF-approximation, on which the data in Tables 10 and 12 are based, only the tangential stress component has been taken into account and variation of differential pressure has not been considered. If the radial stress component is taken into account in a more sophisticated approach of Steiner (denominated as Steiner formula, SF [53]) with otherwise the same data sets, one can observe slight deviations in the variation of the mean hoop stress with clad thickness in Fig. 20, both for the case of normal operation with a constant initial pressure difference of -17 MPa and also for the case of an external pressure drop from 25 to 0 MPa, i.e. an inner pressure of 8 MPa. The latter is important from safety reasons. The comparison shows that the simple KF-approach underestimates slightly the hoop stress values for normal operation and overestimates those for the case of a drop in pressure of the cooling media. The deviations from the SF model are, however, not very significant.

Table 12: Estimated maximum temperatures for different materials for the condition of $R_{M/45,000\,h}$ at 100 MPa and 200 MPa respectively

Material	Stress[+]	Temperature	Reference
MANET II	100	587	FZKA 5722
MANET II	200	512	1996
EURALLOY	100*	553	AGT1-SG2-03
EURALLOY	200*	494	1992
1.4970	100	690	KfK 4217
15Cr-15Ni-Ti	200	629	1986
(sa + cw + a)			
Incoloy 800	100	625	MM Werkstoff-
	200	544	blatt 760
			1976
Inconel 718	100	712	PSB 354
	200	672	1970
PE 16	100	690	AGT1-SG2-1
	200	650	1992

[+] Without any safety margin!

* For equivalent stress level $\overline{\sigma}$ (von Mises)

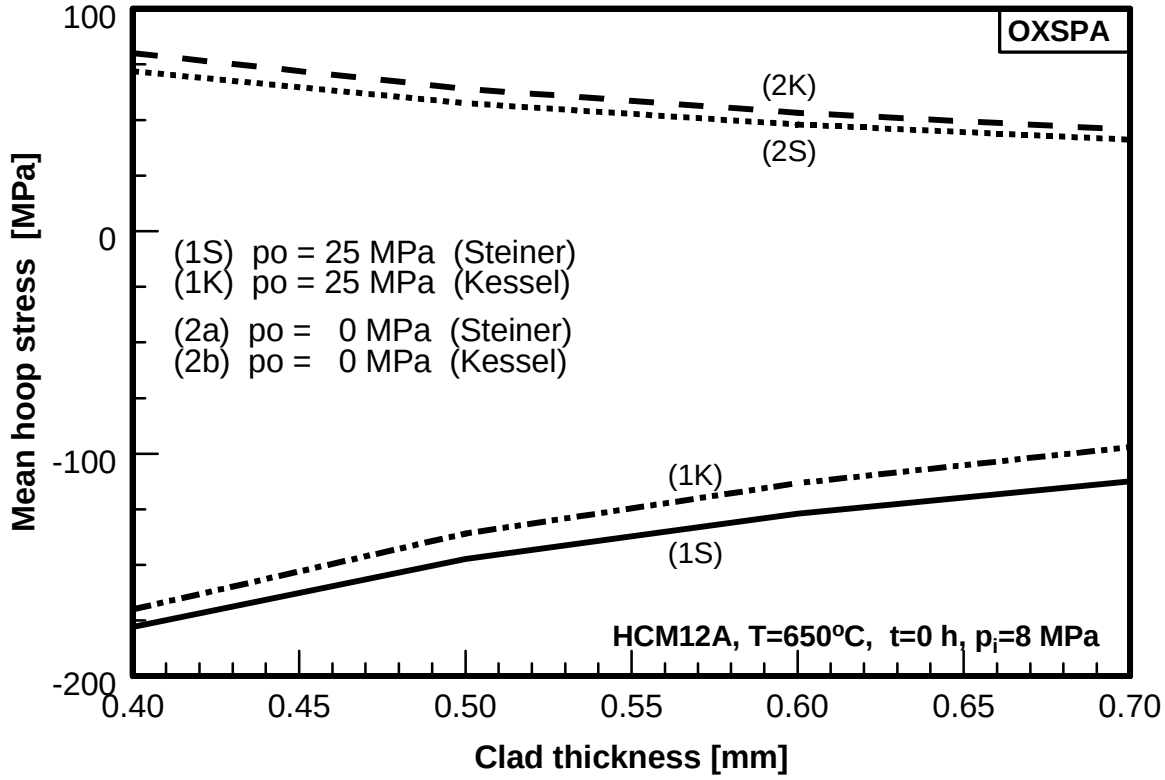

Fig. 20: Hoop stress in dependence of thickness for a cladding outer diameter of 8 mm Curves 1K+1S are the values for the initial pressure difference of 17 MPa and curves 2K+2S represent the data for loss of coolant pressure (Pi= 8 MPa)

Of relevance for the stress development with increasing burnup is however the reduction of wall thickness by inner and outer corrosion and the increase of the inner pressure in fuel pins by fission gas release, which decreases the initial differential pressure Δp with time.

In order to quantify these effects step by step, at first the individual corrosion data for ferritic/martensitic and austenitic stainless steels, compiled and analyzed in Chapter 3, have to be taken into account. They deliver data on oxidation and spallation and can be used in analytical formulas (3 and 4) to determine the metal loss induced by corrosion.

A comparison of oxidation behavior of typical ferritic/martensitic 9-12%Cr like P91 and HCM12A shows that oxidation increases by roughly a factor of two when the chromium content is reduced from 12 to 9 wt-%. This is not unexpected so that – like in conventional steam power plants - a return from the 9%Cr to the group of further

improved 11-12% CrMo(W)VNb steels is envisaged. Another observation is that the contribution of spallation to the reduction of wall thickness is of minor importance, but is included in the calculations.

The oxidation-induced metal loss of conventional 18% Cr- austenitic steels like DIN 1.4910 is comparable to that of the higher alloyed 12% Cr f/m steels like HCM12A, Fig. 21. Therefore, the data of that alloy are assumed to be representative for the ferritic/martensitic as well as for conventional austenitic steels in all further calculations, which is a rather conservative approach for the much improved austenitic stainless steels like TP347HFG.

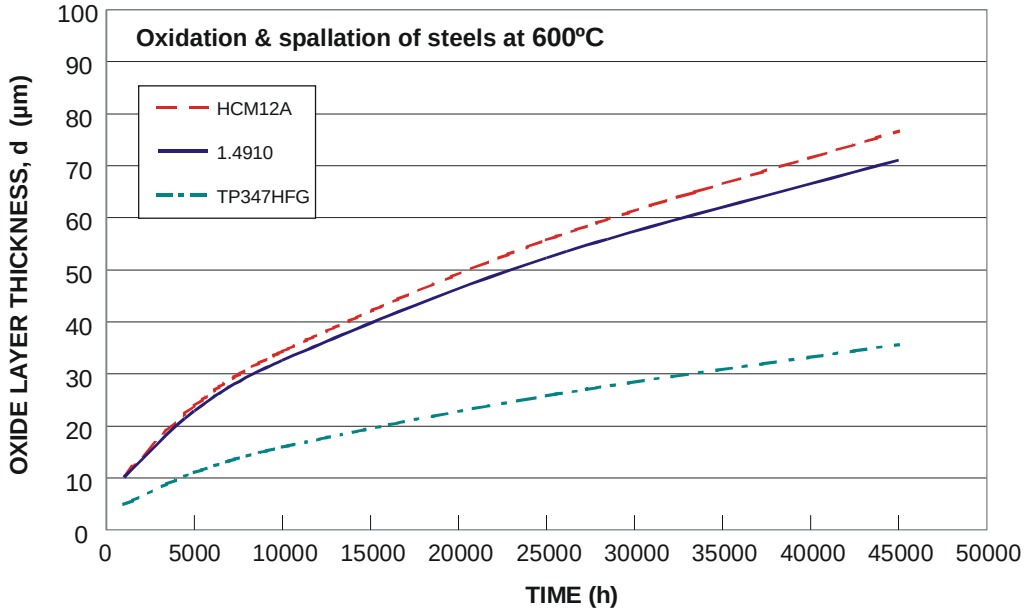

Fig. 21: A comparison of oxidation and spallation for ferritic and austenitic steels at 600°C. Metal loss is half of the oxide thickness.

The second parameter which influences the development of the mean hoop stress in the cladding is the increase of the inner pressure with increasing burnup. A constant fission gas release producing an increase of inner pressure by $2.2 \cdot 10^{-4}$ [MPa h^{-1}] has been adopted as a reasonable value for the model calculations.

With the given data for oxidation and fission gas release it is possible to discriminate which of both effects is the dominant one and how this will affect the previous estimate of the maximum achievable temperature for the candidate materials.

The 9-12% Cr steels have for a hoop stress of 100 MPa a temperature-limit at around 600°C (see Table 12), which is limited by their creep-rupture properties. In Fig. 22 the development of hoop stress with time is calculated with the Steiner formula (SF) for both clad wall thickness values of 0.4 and 0.7 mm. The Figure shows that for this temperature the reduction of differential stress by the buildup of an inner pressure by far exceeds a possible stress increase induced by a reduction of wall thickness due to oxidation. The relative decrease of hoop stress with reduced

differential pressure is smaller for the thicker cladding, as expected. And there is a positive effect of the formed oxide scale on the strength of the cladding. A more detailed explanation of why the formation of a metal oxide scale composite leads to a supportive strength increase of the cladding is given in [53].

In a case like this, where the hoop stress decreases quasi linearly with time one can use an averaged stress level instead of the initial one to determine the maximum achievable temperature, so that compared to the initial values of Table 12 higher maximum allowable temperatures can theoretically be expected. Further below this gain will be estimated.

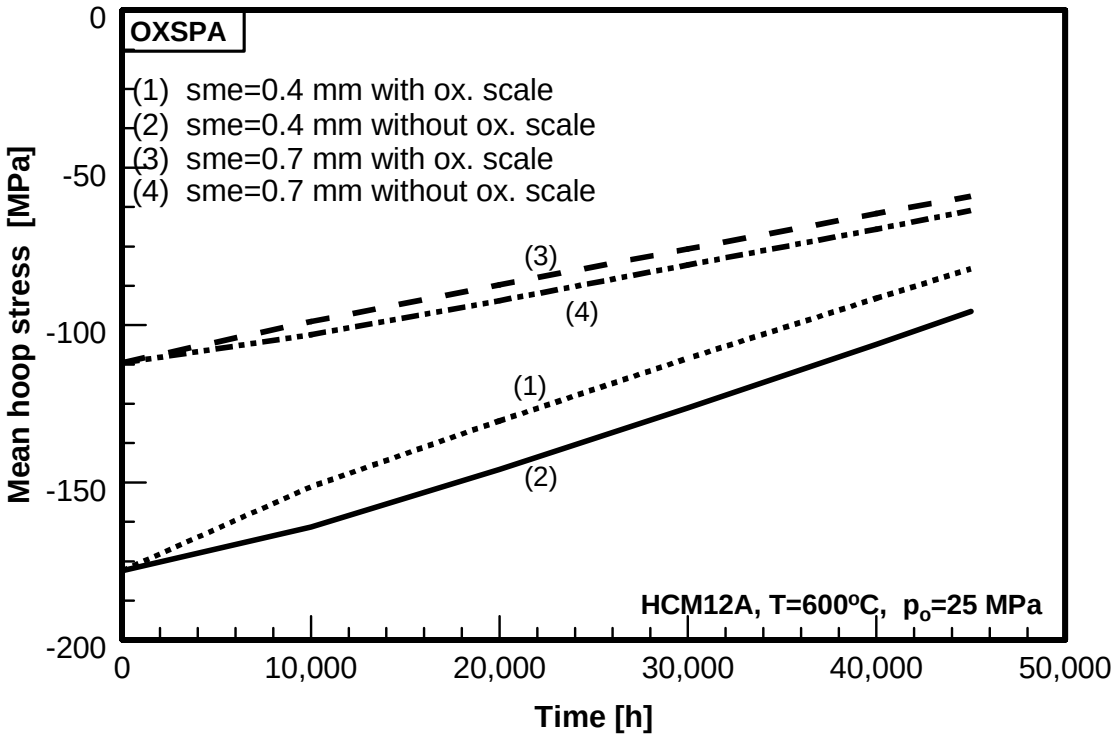

Fig. 22: The evolution of the mean hoop stress in the cladding at 600°C for a wall thickness of 0.4 and 0.7 mm without (2, 4) and with (1, 3) supporting effect of the oxide scale.

The conventional austenitic stainless steels have for $R_{M/45,000h}$ = 100 MPa, a temperature limit ranging from 630 to 690°C, dependent on the composition of the specific alloys. The evolution of the mean hoop stress in dependence of time for 650°C by assuming the same development of differential pressure as above and taking the corrosion data of HCM12A as conservative ones is shown in Fig. 23. Like for the case of the f/m steels in Fig. 22 the decrease of stress in the first 10,000 h induced by the buildup of the fission gas is retarded because of the metal loss by corrosion. The effect is more pronounced because of the higher corrosion rate at 650°C and is of course more visible for a thinner clad. Again the supporting role of the formed oxide scale can be observed.

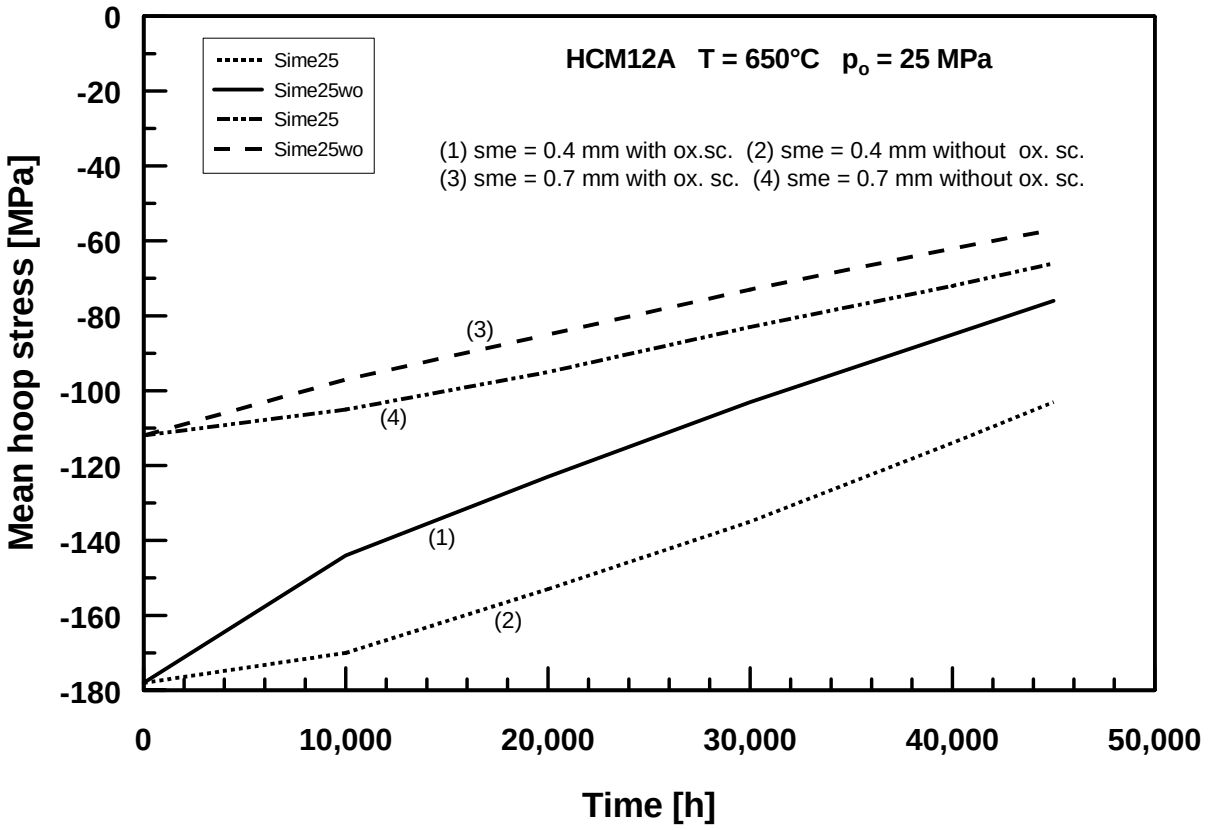

Fig. 23: The evolution of the mean hoop stress in the cladding at 650°C for a wall thickness of 0.4 (1,2) and 0.7 (3,4) mm without (2,4) and with (1,3) supporting effect of the oxide scale.

In Chapter 4, a possible inner corrosion as a function of the burnup has been described in more detail. In the following calculation, it is assumed that the inner corrosion has a parabolic time dependence (Eq. 8), which is the more conservative assumption. A comparison of the effect of outer corrosion alone with the combined effect of inner plus outer corrosion, on the development of the mean hoop stress in Fig. 24 shows that the inner corrosion plays the dominant role. It increases in a first phase the hoop stress and then retards the decrease of the stress level induced by the increasing fission gas release in the cladding. But again the result remains that the effect of decreasing differential pressure exceeds the diminution of clad thickness by outer and inner corrosion.

The question remains whether or not for the f/m and austenitic steels either a higher temperature or a reduced clad thickness could be achieved, if instead of a high initial constant stress, which neither takes into account stress reduction by increasing pin inner pressure nor diminution of clad thickness, a time-averaged pressure, which is based on the actual decrease of hoop stress shown in Fig. 24, is assumed. An estimate of time-averaged stress levels for curves 2 and 4 of Fig. 24 gives values in the range of 80 to 85 % of the initial level and lies therefore in the usual safety margin of stress rupture data, so that for this cladding dimension the initial estimates in Table 12 are on the safe side.

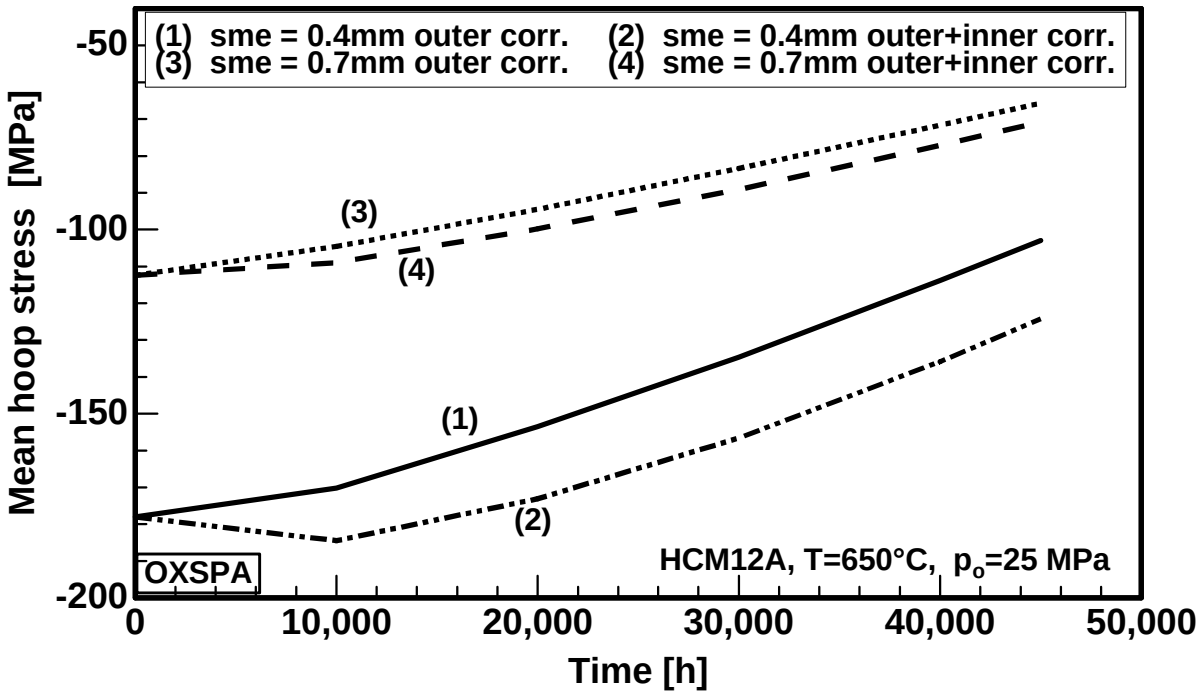

Fig. 24: The evolution of the mean hoop stress in the cladding by comparing the effect of outer corrosion with the combined outer and inner corrosion

For most of the nickel alloys the corrosion by oxidation can be neglected up to 720°C, so that the data given in Tables 10 and 12 are conservative ones. However, as for the other materials, the effect of non-uniform corrosion by sensitization of grain boundaries or stress corrosion cracking are other parameters, which have to be taken into account.

In concluding, the initial estimates of maximum achievable temperatures, based on the creep-rupture properties of the different material groups under the given assumptions must not be revised, if the increase of internal pressure by fission gas release and the metal loss by uniform inner and outer corrosion phenomena are taken into account. However, it is absolutely necessary in a later stage of this study to substitute this analysis by a complete fuel-cladding design, which also has to take into account all other design parameters.

6. Conclusions and proposals for further work

6.1 Operational conditions and recommendations for water chemistry

From the assessment presented above the following conclusions can be drawn:

- The design data proposed for this HPLWR project are very ambitious in comparison with conventional LWR's, especially regarding the cooling medium "supercritical water" in a high pressure system, the temperature range for core materials between 290 and more than 600°C, the extended lifetime and higher burnup of the fuel elements. The much higher neutron and γ-irradiation (up to about 10^{23} n/cm^2 or 60 dpa) which is connected with a higher burnup target and the formation of undesired elements like helium via inelastic nuclear reactions, can change the mechanical and micro-structural properties of in-core materials and negatively influence their dimensional stability. In this respect HPLWR resembles more the operational conditions of a Fast Breeder Reactor than a LWR. Therefore, in the assessment the experience with different material groups under LMFBR conditions is of great importance.

- Regarding the water chemistry to be adapted, it is proposed to use the nearly identical and strict specifications for impurities in the feedwater cycles of conventional LWR power plants in order to minimize in-core deposits, the so-called crud. This is the major aspect for the specification of water chemistry in the HPLWR system since in its core a transition from the sub-to the supercritical state occurs, which is connected with a decrease in solubility of impurities. The compatibility of a basic hydrazine-ammonia chemistry to increase the pH-value, as applied in conventional power plants, with the requirements of the core water chemistry has still to be investigated.

- Radiolysis of the water increases the oxidation potential and hence the risk of electrochemical corrosion. It is expected that the radiolytic water decomposition in an HPLWR will not exceed the normal values observed in a BWR. However, in contrast to the situation in BWR's, where in the upper region of the core steam is generated and hydrogen radicals are stripped away by increasing the concentration of radiolytic oxygen, it is assumed that like in PWR's this problem can be reduced in the HPLWR by the addition of H_2 or by a so-called Noble Chem Technique, by which an enhanced recombination of hydrogen and oxygen is promoted.

- High system pressure can in principle promote general corrosion. Though no consistent data sets for the corrosion behavior of relevant materials in supercritical water are at present available in the open literature, there should be no danger to loose the protective Cr_2O_3-layer formation in steels and Ni-alloys up to at least 650°C due to the high system pressure in HPLWR. Also older data on the corrosion behavior of austenitic stainless steels in a system pressure region varying from 7-35 MPa do not suggest greater effects of increasing pressure on corrosion.

- The sensitivity to stress corrosion cracking is dependent on the water chemistry (oxygen and chlorine concentration) and the selected materials. A rigorous limitation of the dangerous additives oxygen and chlorides in the specification of

water chemistry is therefore absolutely mandatory. Regarding the materials choice, it is well known that especially austenitic stainless steels on one side and Ni-alloys are sensitive to this effect. However, by an appropriate material composition like an intermediate Ni content, a low carbon concentration or the use of Nb/Ti stabilized alloys, the sensitivity to general SCC and IGSCC can be reduced.

- A possible problem area for in-core cladding materials is the relatively high stress level (≥ 100MPa) at elevated temperature under irradiation, where either irradiation creep or radiation-enhanced thermal creep could occur. Dependent on the acting deformation mechanism, a reduction of the thermal creep rupture properties has to be envisaged.

6.2 Selection of ex-vessel and cladding (in-core structural) materials

Ex-vessel materials

Based on the presented data for oxidation the following selection of out-of-core materials can be recommended. The order is increasing with the oxidation resistance:

P91 > > HCM12A / 1.4910 > TP347HFG > Incoloy 800 > IN 625

The fact that Ni-based alloys are not favorable under irradiation, the austenitic steel types of TP347HFG and 1.4910 are the most promising. In comparison of general experience, manufacturing properties and the resistance for e.g. cyclic loading, the ferritic/martensitic steels in general and especially HCM12A may show a high potential as well. Some main features are summarized:

- In the group of 9-12% Cr F/M-steels the candidate materials are P91 and HCM12A. For these steels a good technological basis is available. The oxidation rate of HCM12A corresponds to that of conventional 18Cr-10 Ni austenitic stainless steels.

- The selected type austenitic alloys are 1.4910 and TP347HFG. The steel TP347HFG is superior in respect to the oxidation resistance. The effect of thermal cycling has to be investigated with special care in the future due to the high susceptibility for spallation during thermal shocks. This is due to the large mismatch of thermo-physical properties between austenitic steels and oxides.

- The IN625, a Ni-based superalloy, has a negligible oxidation rate in steam. However, the problems under irradiation due to the high alloying will become a limitation.

Cladding (Core structural materials)

The analysis of the different material groups for cladding application investigated in this report is based on their creep-rupture strength and on their general corrosion properties. The assessment concludes that for an estimated upper temperature of

650°C, not only Ni-alloys but also austenitic stainless steels can be envisaged. If specific items like neutron absorption or the sensitivity to helium embrittlement and stress corrosion cracking are taken into account, the following material groups should be considered with priority as cladding and eventually as core structural materials.

- Austenitic stainless steels of type Fe-(15-18%)Cr-(10-15%)Ni-Mo-V-Ti/Nb. A typical representative of this class for cladding application is the alloy X10CrNiMoTiB 15 15 (DIN 1.4970). Alloy 1.4550 has proven as a good choice for core structural application.

- Higher Cr-Ni-containing steels like Incoloy 800 (Fe-20Cr-35Ni-Ti) are another alternative with improved corrosion properties, but they would need improved strength.

- Existing ferritic/martensitic steels of type 9-12% CrMoV(Nb) like DIN 1.4914 or 1.4922 and P91 or their “low activation” variants like EUROFER are presently limited to an upper temperature of 600°C. However, in the long-term oxide-dispersion strengthened (ODS) f/m steels like EUROFER-ODS, or higher 13-15 % Cr-containing ferritic steels should be considered as attractive alternatives, provided that ductile-to-brittle transition temperature (DBTT) after irradiation lies well below the core inlet temperature.

6.3 Proposals for future work

- The assessment has shown that the most uncertain area in the analysis is the corrosion behavior of materials under supercritical water conditions and a possible influence of a high stress level on stress corrosion cracking phenomena. Therefore, CEA, FZK and VTT propose to perform studies in autoclaves (CEA) and instrumented loop experiments (VTT, FZK) on corrosion and stress corrosion under well-defined water chemistry and stress conditions. FZK intends to investigate the influence of gaseous, low oxygen environment on the creep-rupture and creep buckling properties in the typical HPLWR σ-ε-T parameter range. Detailed descriptions of the research proposal can be found in the attachments to reference [54].

- A detailed assessment of other in-core and out-of-core materials in special components like the RPV, general core structures, turbine and piping materials has to be started or continued

- For the cladding materials in future HPLWR’s the proposed class of recommended austenitic stainless steels has to be further optimized with regard to the type and degree of stabilization, the necessary carbon content and the balance between chromium, nickel and minor alloying elements to achieve an optimum in creep-rupture strength and corrosion resistance, including stress corrosion cracking.

- The deformation mechanisms under irradiation in the overlapping region of irradiation-creep and radiation-enhanced thermal creep have to be investigated.

- On a long term the development of reduced-activation (9-12% Cr) ferritic/martensitic steels or (14-18% Cr) ferritic steels with emphasis on ODS-variants with strongly improved high temperature creep-rupture properties and lower DBTT should be envisaged. With these alloys maximum cladding temperatures of 700°C seem to be possible.

- All these activities should be part of a Key Technology Phase to be started in the next European Framework Programme of HPLWR.

7. References

[1] D. Squarer, private communication

[2] Y.Oka, K. Dobashi, S. Koshizuka, ICONE 6, Proc. on the 6th Internat. Conf. on Nuclear Engineering, San Diego, Calif., May 10-15, 1998

[3] D. Bittermann; Framatome ANP, private communication

[4] E. Metcalf, B. Scarlin, Advanced High Efficiency Steam Power Plants, Proceedings of the 6th Liege Conf., Forschungszentrum Jülich, "Materials for Advanced Power Engineering 1998", Parts I-III, Vol. 1, p. 35

[5] K. Ehrlich, J. Konys, private communication

[6] J. Konys, private communication

[7] G. Rimpault, E. Testa, private communication

[8] A. Tanskanen, F. Wasastjerna, Neutronics calculations for HPLWR cladding material selection, Technical note at the Chatou Meeting, March 4-6, 2002. VTT Processes, Project Report YE-PR-13/02

[9] VGB-Richtlinie für das Wasser in Kernkraftwerken mit Leichtwasserreaktoren, VGB-R 401 J, 2nd edition 1985, Verlag technisch-wissenschaftlicher Schriften, Essen, Germany

[10] Revision der VGB-Richtlinie für das Wasser in Kernkraftwerken mit Leicht-wasserreaktoren (VGB-R 401 J), VGB Kraftwerkstechnik 76 (1996), Heft 3

[11] F. Garzarolli, R. Holzer, Waterside corrosion performance of light water power reactor fuel, Nucl. Energy 31, No. 1 (1992) 65

[12] VGB Guidelines for boiler feedwater, boiler water and steam of steam generators with a permissible operating pressure > 68 bar, VGB-R 450 Le, Edition 1995, Verlag technisch-wissenschaftlicher Schriften, Essen, Germany

[13] M. E. Shitsman, EPRI target values: Thermal Engineering Vol. 47/7 p 606-611, EPRI TR-105041, 1996

[14] G. P. Marsh, K. J. Taylor, G. Bryan, S. E. Worthington, The influence of radiation on the corrosion of stainless steel, Corrosion Science Vol. 26, No. 11 (1986) 971

[15] Materials for Advanced Power Engineering 1998, Proceedings of the 6th Liege Conference, Parts I-III, Eds.: J. Lecomte-Beckers, F. Schubert and P.J. Ennis, Forschungszentrum Jülich, 1998 Germany

[16] Proceedings on Baltica IV: Plant Maintenance for Managing Life & Performance, VTT Symposium 184. VTT-Espoo, Finland 1998, p. 13–27

[17] R. L. Klueh, Future Directions for Ferritic/Martensitic Steels for Nuclear Applications, Proc. of SCR-2000: Nov. 6-8, 2000, Tokyo, Japan, Paper 403

[18] R. U. Husemann; VGB Kraftwerkstechnik 9,1999, p. 84-87

[19] Advanced Steam Plant, May 1997, London, p. 3-16, I. Mech. E. Conference Transaction (1997), C522/030/97

[20] J. Konys, S. Fodi, J. Haußelt, H. Schmidt, V. Casal, Corrosion of high temperature alloys in chloride containing supercritical water oxidation systems, Corrosion 55 (1999) 45

[21] J. Konys, A. Ruck, J. Novotny, J. Haußelt, Corrosion of nickel based alloy G-30 between 100 and 420°C, pH values from 2 to 6 and pressures ranging from 250 to 480 bar under conditions of supercritical water oxidation, CORROSION/2001, Houston, Texas, USA, March 11-16, 2001, paper 01366

[22] L. B. Kriksunov, D. D. Macdonald, Phenomenological analysis of corrosion phenomena in supercritical water oxidation systems, 1st Int. Workshop on Supercritical Water Oxidation, February 6-9, 1995, Jacksonville, Florida, USA

[23] P. B. Longton, TRG-Report 1144C (1966)

[24] W. K. Boyd, H. A. Pray, Corrosion of stainless steels in supercritical water, Corrosion NACE, Vol. 13 (1957) 375

[25] C. Liu, L. B. Kriksunov, D. D. Macdonald, Electrochemical noise analysis for monitoring corrosion activity in SCWO systems, 1st Int. Workshop on Supercritical Water Oxidation, February 6-9, 1995, Jacksonville, Florida, USA

[26] N. Boukis, R. Landvatter, W. Habicht, G. Franz, S. Leistikow, R. Kraft, O. Jacobi, First experimental SCWO corrosion results of Ni-base alloys fabricated as pressure tubes and exposed to oxygen containing diluted hydrochloric acid at T≤450°C, P=24 MPa, 1st Int. Workshop on Supercritical Water Oxidation, February 6-9, 1995, Jacksonville, Florida, USA

[27] M. Modell, Critical perspectives on the development and potential applications of SCWO, 1st Int. Workshop on Supercritical Water Oxidation, February 6-9, 1995, Jacksonville, Florida, USA

[28] G. J. Rittenmyer, Terminal examination and evaluation of EVESR Mark II annular superheat fuel, GEAP-5510, July 1967, AEC-Research and Development Report

[29] S. A. Rabin, Terminal examination and evaluation of EVESR Mark III rod cluster superheat fuel, GEAP-5481, June 1967, AEC-Research and Development Report

[30] R. U. Husemann, VGB Kraftwerkstechnik 10,1999, p. 146-149

[31] Y. Fukuda, K. Tamura and T. Sato, Steam oxidation properties of high Cr ferritic steels. in Ref. [8] Paper 402

[32] Proceedings on VGB-ESKOM International Material Conference, 18. - 20.9.2000, Pretoria, South Africa

[33] R. Knödler and P. J. Ennis, Oxidation of high-strength ferritic steels in steam at 650°C; Proceedings BALTICA V, VTT Symposium 211, VTT-Espoo, Finland 2001, p. 355-364

[34] W. L. Pearl, E. G. Brush, G. G. Gaul, S. Leistikow, General Corrosion of Inconel Alloy 625 in Simulated Super-heated Reactor Environment. Nuclear Applications Vol. 3, July 1967, p. 418-432

[35] W. L. Pearl, E. G. Brush, G. G. Gaul, G. P. Wozadlo, General Corrosion of Incoloy 800 in Simulated Superheated Reactor Environment. Nuclear Applications Vol. 1, June 1965, p. 235-245

[36] S. Leistikow, et al.; KFK-Report 2033, Karlsruhe, Germany, December 1974

[37] J. Blanchet, H. Coriou, Proc. of the Petten Int. Conf. ”Alloy 800”, March 14-16, 1978) Ed. By W. Betteridge, North-Holland Pub. Co., (1978) p. 241-262

[38] R. A. Page, A. McMinn, Relative stress corrosion susceptibilities of alloys 690 and 600 in simulated boiling water reactor environments, Met. Trans. A Vol. 17A May 1986, p. 877

[39] M. Erve, U. Wesseling, R. Kilian, R. Hardt, G. Brümmer, V. Maier, U. Ilg, Cracking in stabilized austenitic stainless steel piping of German boiling water reactors, Nucl. Eng. Des. 171 (1997) p. 113-123

[40] O. Wachter, U. Wesseling, J. Bruns, R. Kilian, Interkristalline Spannungsrißkorrosion an Nb-stabilisiertem austenitischem Stahl in Kerneinbauten eines Siedewasserreaktors, VGB Kraftwerkstechnik 76 (1996) Heft 6, p. 514-520

[41] L. Fournier, privat communication

[42] R. L. Klueh, D. R. Harries, High-chromium ferritic and martensitic steels for nuclear applications, ASTM 2001, Chapter 5, p 56-62

[43] C. Brown, K. Ehrlich, V. Levy, et al., Cladding and Wrapper Development for Fast Reactor High Performance, Int. Conf. on Fast Reactors and Related Fuel Cycles; Kyoto, J, October 28 - Nov. 1, 1991, Tokyo: Atomic Energy Soc. of Japan

[44] A. Hishinuma, A. Kohyama, R. L. Klueh, D. S. Gelles, W. Dietz, K. Ehrlich, Current status and future R and D for reduced-activation ferritic/martensitic steels, Proc. of the 8th Int. Conf. on Fusion Reactor Materials, Sendai, Japan, October 26-31, 1997, Part A, 193-204, Journal of Nuclear Materials, p. 258-263 (1998)

[45] K. Ehrlich, R. Lindau, A. Möslang, M. Schirra, EUROFER-97 and development strategy for the RAFM steels in Europe, IEA-Working Group Meeting on Ferritic/Martensitic Steels, Tokyo, Japan, November 2-3, 2000

[46] H. J. Bergmann, W. Dietz, K. Ehrlich, G. Mühling, M. Schirra, Entwicklung des Werkstoffs X10CrNiMoTiB 1515 als Strukturmaterial für Brennelemente FZKA-6864, Juni 2003

[47] E. Tenckhoff, M. Erve, Materials for nuclear power plants in Western countries, Atomwirtschaft, April 1992, p. 185-192

[48] M. L. Großbeck, K. Ehrlich, C. Wassilew, An assessment of tensile, irradiation creep, creep-rupture and fatigue behaviour in austenitic stainless steels with emphasis on spectral effects, Proc. of the Int. Workshop on Radiation Damage Correlation for Fusion Conditions, Silkeborg, DK, September 28 - October 3, 1989, Journal of Nuclear Materials, 174 (1990), p. 264-81

[49] R. Hübner; Das Bestrahlungsverhalten des austenitischen Stahls 1.4970, FZKA 6372, Juni 2000

[50] W. Dienst, V. Gibs , O. Götzmann, Werkstoffe und Korrosion 33 (1982) p. 533-541

[51] V. Gibbs, KfK-Bericht 3283, Oktober 1983

[52] A. Yamaji, Y. Oka, S. Koshizuka, private communication

[53] H. Steiner, Stress effects in cylindrical tubes of austenitic and ferritic/ martensitic steels with oxide scales, FZKA-Report 6737, November 2002

[54] D. Squarer, private Communication